



HAL
open science

Multi-mode propagation and diffusion analysis using the three-dimensional second strain gradient elasticity

Bo Yang, Mohamed Ichchou, Abdelmalek Zine, Christophe Droz

► To cite this version:

Bo Yang, Mohamed Ichchou, Abdelmalek Zine, Christophe Droz. Multi-mode propagation and diffusion analysis using the three-dimensional second strain gradient elasticity. *Mechanical Systems and Signal Processing*, 2023, 10.1016/j.ymssp.2022.109970 . hal-03879291

HAL Id: hal-03879291

<https://hal.science/hal-03879291>

Submitted on 30 Nov 2022

HAL is a multi-disciplinary open access archive for the deposit and dissemination of scientific research documents, whether they are published or not. The documents may come from teaching and research institutions in France or abroad, or from public or private research centers.

L'archive ouverte pluridisciplinaire **HAL**, est destinée au dépôt et à la diffusion de documents scientifiques de niveau recherche, publiés ou non, émanant des établissements d'enseignement et de recherche français ou étrangers, des laboratoires publics ou privés.

Multi-mode propagation and diffusion analysis using the three-dimensional second strain gradient elasticity

Bo Yang^a, Mohamed Ichchou^{a,*}, Abdelmalek Zine^b, Christophe Droz^c

^a*LTDS - CNRS UMR 5513, Vibroacoustics & Complex Media Research Group, École Centrale de Lyon, France*

^b*Institute Camille Jordan – CNRS UMR 5208, École Centrale de Lyon, France*

^c*Univ. Gustave Eiffel, Inria, COSYS/SII, I4S Team, France*

Abstract

The multi-mode propagation and diffusion properties are crucial informations when studying complex waveguides. In this paper, firstly, the three-dimensional modeling of micro-sized structures is introduced by using the second strain gradient theory. The constitutive relation is deduced while the six quintic Hermite polynomial shape functions are employed for the displacement field. The weak formulations including element stiffness and mass matrices and the force vector are calculated through the Hamilton's principle and the global dynamic stiffness matrix of a unit cell is assembled. Then, free wave propagation characteristics are analyzed by solving eigenvalue problems within the direct wave finite element method framework. The dispersion relations of positive going waves considering the size effects are illustrated. Furthermore, the effects of higher order parameters on the dispersion curves are discussed and the forced responses with two boundary conditions are expounded. Eventually, the wave diffusion including reflection and transmission coefficients are illustrated through simple and complex coupling conditions, respectively. The dynamic analysis of coupled waveguides through the wave finite element method equipped with the second strain gradient is a novel work. The results show that the proposed approach is of significant potential for investigating the wave propagation and diffusion characteristics of micro-sized structures.

Keywords: Wave finite element method; Second strain gradient theory; Wave propagation; Wave diffusion

1. Introduction

The dynamical properties of guided waves such as dispersion and diffusion have been widely studied over the past decade especially in the field of acoustics, earthquake and electromagnetics. Evaluating and optimizing the vibration characteristics of waveguides is of great significance in engineering applications. Initially, studies focused on the guided waves interaction at interfaces or at boundaries between different macro-mediums. For instance, Mace [1] analyzed the diffusion properties of two coupled homogeneous beams. The result shows that incident near fields can give rise to substantial propagating components. Mencik and Ichchou [2] studied the multi-mode propagation and diffusion in periodic structures. A classification criterion was offered in their work enabling a rigorous identification of guided modes. Currently, the experimental studies on the dynamic characteristics of guided waves have also attracted the attention of many scholars. For example, Taleb et al. [3] conducted an experiment of wave propagation inside an impact damage region and identified the propagating modes along the plate structure. Herrero et al. [4] reported an experimental research of an Helmholtz resonators. The proposed structure shows experimentally a quasi-perfect sound absorption in the range of frequencies of interest, which is in good agreement with the theoretical predictions.

Usually, the macro-structures mentioned above are simple geometries and are assumed to be isotropic and homogeneous. In these structures, the local behavior of internal heterogeneity plays a major role in their vibration properties within the Classical Theory (CT) of continuum mechanics [5] framework. But for the micro-sized structures with size effects, their structural properties are different from macro-sized structures. Generally, there exist three major aspects

*Corresponding author: mohamed.ichchou@ec-lyon.fr

of size effects namely large surface-volume ratio, micro-deformations and non-local interaction, which are explained as follows: firstly, the micro-particles such as atoms with associated energy on the surface of the structure produce surface tension which can not be ignored in micro-structures [6, 7, 8]. Secondly, in addition to the macro-deformations caused by macro-material in the structure, the micro-deformations such as micro-rotation, micro-stretch caused by micro-material in the structure have important influences on the mechanical behavior of the structure [9, 10, 11]. Lastly, besides the local interaction property, there exist a non-local interaction property in the micro-sized structure [12, 13, 14]. The wave propagation and diffusion in micro-medias can no longer be reasonably predicted by CT.

In order to interpret the properties of micro-sized structures caused by the size effects mentioned above, the non-classical continuum theories of elasticity have been proposed. Generally, these non-classical theories can be categorized into non-local elasticity theory [15, 16], micro-continuum theory [17, 18], surface elasticity theory [19, 20] and strain gradient family [21, 22, 23]. The strain gradient family is composed of the couple stress theory [24, 25, 26], the First Strain Gradient (SG) theory [27, 28], the Second Strain Gradient (SSG) theory [29, 30] and the modified couple stress theory [31, 32, 33]. Mindlin established one of the strain gradient families called the SG theory, in which the constitutive relations are composed of strain and the first gradient of strain. The atomic structure with the nearest and next nearest interactions between different particles is used to describe the SG theory in the framework of lattice spring models, but only in non-centrosymmetric materials [34]. In order to explore the properties of centrosymmetric materials, the SSG theory [29, 35] was put forward, which offers a reasonable description of the strain and surface tension properties on the micro-structure's surface by introducing the high-order parameters. The constitutive relations in the SSG theory are functions of strain, first and second gradient of strain. There are three major advantages of using the SSG theory: firstly, higher order deformations caused by higher order characteristic length can be confirmed. Secondly, the stiffness hardening phenomenon caused by non-local or long-range interaction can be explained. Lastly, the special mechanical properties of the micro-sized structures such as the stiffness hardening phenomenon are mainly manifested in high frequency. These special characteristics can be effectively explored by using the SSG theory.

Recently, researchers have conducted some explorations on dynamic properties of micro-sized structure through strain gradient analytical theories. For example, Lim et al. [36] derived new dispersion relations in Euler–Bernoulli and Timoshenko nano-beams based on the strain gradient theory. The stiffness of nano-beams matches the experimental observation. Dario and Askes [37] studied the flexural wave propagation characteristics in carbon nano-tubes by a strain gradient beam theory. The significant improvements in the prediction of flexural wave dispersion are achieved by a new three-length-scale gradient elasticity formulation. For the 1D wave diffusion, Zhu et al. [38] illustrated wave transmission and reflection coefficients within the SSG theory framework. Torabi et al. [39, 40] introduced the dynamical properties of nano-structures according to the strain gradient theory. It shows that the increase of thickness-to-material length scale ratio leads to the decrease of the non-dimensional frequencies.

On the other hand, in order to study the wave dispersion and diffusion in complex structures, numerical methods such as Spectral Finite Element (SFE) method [41] and Semi-Analytical Finite Element (SAFE) [42] can be used. In the past decade, the Wave Finite Element Method (WFEM) [43, 44, 45, 46] has attracted many works. The advantage of WFEM is the convenient application in the engineering field. Since it can be developed from the Finite Element Method (FEM) packages, which allows the current element library and grid generation procedures to be applied for the modeling of different waveguide structures. In addition, WFEM can reduce a global periodic structure into a single substructure or unit cell based on the periodic structures theory [47, 48]. The resulting stiffness and mass matrices are post processed to offer the dynamic stiffness matrix. The dynamical properties of the periodic structure can be reflected through the spectral analysis of the unit cell [49, 50].

Adaptations of the WFEM framework to the strain gradient theories were proposed in authors' previous works: Yang et al. [51] studied 1D bending and torsion wave propagation characteristics by combining the SSG theory and the 1D WFEM for the first time. Then, Yang et al. [52] explored the 2D wave propagation in a periodic beam grid within the 2D WFEM framework based on the SSG theory. On the other hand, Reda et al. [53] analyzed the 3D wave propagation properties of the 3D periodic structure through the homogenized strain gradient theory. To the authors' knowledge, WFEM has never been exploited to investigate wave diffusion characteristics between the coupled SSG waveguides. In addition, there exist complex waves such as higher order waves in realistic periodic structures. So, the exploration of multi-mode propagation and diffusion in complex structures is of great significance. Meanwhile, predicting the wave diffusion properties including reflection and transmission through different coupling interfaces by combining the SSG theory and WFEM is a novel work.

The main objective of this work is, firstly, to investigate the multi mode propagation in a 3D periodic waveguide by the SSG theory, analyze the influence of high-order parameters on dispersion relation, study the forced response of the waveguide, and, secondly, to confirm the wave diffusion under a simple coupling condition and a complex coupling condition. The reason for combining the SSG theory with WFEM is that the size-dependent characteristics of micro-sized medias can be interpreted by the SSG theory and the dynamical properties of complex periodic structures can be investigated through WFEM.

In order to explore the dynamical behaviors as mentioned above for the 3D waveguide structure, this article begins with the derivation of constitutive relations of 3D model based on the SSG theory. The six-term polynomial function is used to determine the high order shape function and the 3D element stiffness and mass matrices are deduced by using Hamilton's principle in the time domain. Then, the free wave propagation is analyzed by solving the direct Bloch formulation. The wave diffusion is confirmed through a simple coupling condition and a complex coupling condition. In this work, the wave diffusion includes reflection coefficients (\mathbf{R}) and transmission coefficients (\mathbf{T}), where \mathbf{R} is defined as the negative-going wave amplitudes at the left surface of coupling element, \mathbf{T} is defined as the positive-going wave amplitudes at the right surface of coupling element[54]. The simple coupling condition can be explained as: the wave modes calculation in waveguides and coupling element are based on the same theory (SSG-SSG or CT-CT). The degrees of freedoms (DOFs) on the left side of the coupling surface are equal to the ones on the right side of the coupling surface. The length of the coupling element along the x direction is short, which means that the waves don't delay in the coupling element. On the other hand, the complex coupling condition can be introduced as: the wave modes calculation in waveguides is based on the CT instead of the SSG theory in the coupling element (CT-SSG). The DOFs on the left side of the coupling surface are not equal to the ones on the right side of the coupling surface. In order to ensure the consistency of the DOFs on the left and right sides of the coupling surface, extra unknown higher order displacements and forces vectors need to be considered in the waveguides modeling. The length of the coupling element along x is long, which means that there exist wave propagation constant and the waves delay in the coupling element. As discussed by Placidi et al. [55], there exist four types of connections between two sides of the interface boundary, namely the "generalized internal clamp", the "generalized internal hinge", the "generalized internal roller" and the "generalized internal free end". In our work, the boundary condition on the coupling element interface is assumed as: the displacement and the derivative of displacement (also called higher order displacement) remain continuous on the two sides of coupling interface, which is same as the "generalized internal clamp" condition.

The article's structure is the following: in section 2, the constitutive relations of 3D micro-sized models are introduced in the SSG theory framework and the weak formulations including element stiffness and mass matrices and the force vector are calculated. Afterwards, in section 3, free wave propagation characteristics are expressed by solving eigenvalue problems in the direct WFEM framework, and diffusion matrices for simple coupling condition and complex coupling condition are confirmed. In section 4, wave dispersion and diffusion, effects of higher order parameters, and forced response are introduced. Finally, some useful conclusions are presented in section 5.

2. Second Strain Gradient (SSG) theory for 3D models

In this section, the constitutive relations of 3D micro-sized model are introduced in the SSG theory framework firstly. Then, the displacement vector is derived by employing the six quin-tic Hermite polynomial shape function. Finally, the weak formulations including element stiffness, mass matrices and force vector are calculated using the Hamilton's principle.

2.1. Constitutive relations

The strain energy density $\overline{\mathcal{U}}$ composed of strain $\boldsymbol{\varepsilon} = \text{sym}(\nabla \mathbf{U})$, first gradient of strain $\boldsymbol{\xi} = \nabla \boldsymbol{\varepsilon}$ and second gradient of strain $\boldsymbol{\zeta} = \nabla \nabla \boldsymbol{\varepsilon}$ in the SSG theory framework was put forward by Mindlin [29], as below:

$$\begin{aligned} \overline{\mathcal{U}} = & \frac{1}{2} \lambda \boldsymbol{\varepsilon}_{ii} \boldsymbol{\varepsilon}_{jj} + \mu \boldsymbol{\varepsilon}_{ij} \boldsymbol{\varepsilon}_{ij} + a_1 \boldsymbol{\xi}_{ijj} \boldsymbol{\xi}_{ikk} + a_2 \boldsymbol{\xi}_{iik} \boldsymbol{\xi}_{kjj} + a_3 \boldsymbol{\xi}_{iik} \boldsymbol{\xi}_{jjk} + a_4 \boldsymbol{\xi}_{ijk} \boldsymbol{\xi}_{ijk} + a_5 \boldsymbol{\xi}_{ijk} \boldsymbol{\xi}_{jki} + b_1 \boldsymbol{\zeta}_{iijj} \boldsymbol{\zeta}_{kkll} \\ & + b_2 \boldsymbol{\zeta}_{ijkk} \boldsymbol{\zeta}_{ijll} + b_3 \boldsymbol{\zeta}_{iijk} \boldsymbol{\zeta}_{jkll} + b_4 \boldsymbol{\zeta}_{iijk} \boldsymbol{\zeta}_{llkj} + b_5 \boldsymbol{\zeta}_{iijk} \boldsymbol{\zeta}_{lljk} + b_6 \boldsymbol{\zeta}_{ijkl} \boldsymbol{\zeta}_{ijkl} + b_7 \boldsymbol{\zeta}_{ijkl} \boldsymbol{\zeta}_{jkli} + c_1 \boldsymbol{\varepsilon}_{ii} \boldsymbol{\zeta}_{jjkk} \\ & + c_2 \boldsymbol{\varepsilon}_{ij} \boldsymbol{\zeta}_{ijkk} + c_3 \boldsymbol{\varepsilon}_{ij} \boldsymbol{\zeta}_{kkij}. \end{aligned} \quad (1)$$

where \mathbf{U} is the displacement vector, symbol ∇ means the gradient operator, λ and μ represent the *Lamé* parameters which are related to the Young's modulus E , the Poisson's ratio ν and the shear modulus G , as $\mu=G=E/2(1+\nu)$, $\lambda=\nu E/(1+\nu)(1-2\nu)$. a_i , b_i and c_i denote the higher order parameters in the SSG theory, which can be confirmed via the inter-atom potential function method [34]. On the other hand, there exist other methods for the identification of higher order parameters that are valid for larger length scales. For example, Barchiesi et al. [56] calculated these parameters in the framework of finite deformations using granular micromechanics assumptions and Piola's ansatz for discrete-continuum identification. In our work, the Face-Centered Cubic (FCC) materials Aluminum (Al) and Copper (Cu) are used. The size of a single anisotropic crystal unit can be described through the lattice parameter a_0 [57], whose value for different materials is presented in Sec.4. In a single crystal of a material, the physical and mechanical properties often differ with orientation. Even if the individual grains are anisotropic, the property differences tend to average out and, overall, the material is isotropic. So, anisotropy refers to the microscopic properties of a single crystal, while isotropy refers to the macroscopic properties of a material composed of a large number of crystals. In order to use the isotropic formulation reasonably and make sure the structure macroscopically isotropic, in this paper, the size of the structure as shown in Sec.4 is defined much larger than a crystal unit.

Based on the 3D elasticity theory, the vector of the displacement field defined in the Cartesian coordinate system (x, y, z) is given as:

$$\mathbf{U}(x, y, z, t) = \begin{pmatrix} u_1(x, y, z, t) \\ u_2(x, y, z, t) \\ u_3(x, y, z, t) \end{pmatrix}, \quad (2)$$

where u_1 , u_2 and u_3 are the the displacements along x , y and z direction.

The relations between strains and displacement components can be defined by introducing the vectors of first, second and third order derivatives of displacement components:

$$\boldsymbol{\varepsilon} = \boldsymbol{\Psi}_1 \mathbf{U}, \quad \boldsymbol{\xi} = \boldsymbol{\Psi}_2 \mathbf{U}, \quad \boldsymbol{\zeta} = \boldsymbol{\Psi}_3 \mathbf{U}, \quad (3)$$

where $\boldsymbol{\Psi}_1$, $\boldsymbol{\Psi}_2$ and $\boldsymbol{\Psi}_3$ are addressed in Appendix A.

Then, the constitutive relations for the 3D model by the SSG theory can be defined as:

$$\boldsymbol{\tau}_1 = \mathbf{L}\boldsymbol{\varepsilon} + \mathbf{C}\boldsymbol{\zeta}, \quad \boldsymbol{\tau}_2 = \mathbf{A}\boldsymbol{\xi}, \quad \boldsymbol{\tau}_3 = \mathbf{B}\boldsymbol{\zeta} + \mathbf{C}^T \boldsymbol{\varepsilon}, \quad (4)$$

in which the details of matrices \mathbf{L} , \mathbf{A} , \mathbf{B} and \mathbf{C} are presented in Appendix A. Finally, the strain energy density for the SSG theory can be rewritten as the matrix form:

$$\overline{\mathcal{U}} = \frac{1}{2} (\boldsymbol{\varepsilon}^T \boldsymbol{\tau}_1 + \boldsymbol{\xi}^T \boldsymbol{\tau}_2 + \boldsymbol{\zeta}^T \boldsymbol{\tau}_3). \quad (5)$$

2.2. Discretization and element matrices

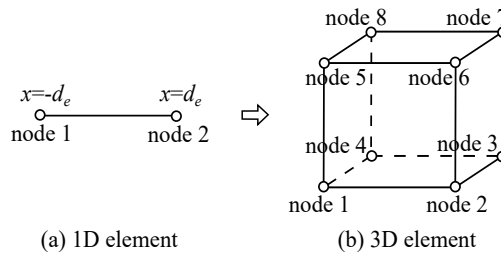


Fig. 1: The 1D and 3D Hermite elements with C^2 continuity. d_e is the half length of the 1D element.

After obtaining the strain energy density, the next step is to calculate the weak form including stiffness and mass matrices and force vector. The 1D and 3D Hermite elements are shown in Fig.1. The node DOFs $\overline{\mathbf{u}}_1^{(e)}$ for the 1D element and the node DOFs $\mathbf{u}_1^{(e)}$ for the 3D element are presented in Appendix A. Firstly, in order to ensure the

continuity of higher derivatives up to the second order between 1D elements, the six-term polynomial function is considered to interpolate the scalar field $U_1=u_1(x, t)$ inside a 1D element, as follows:

$$U_1 = \begin{bmatrix} 1 & x & x^2 & x^3 & x^4 & x^5 \end{bmatrix} \begin{bmatrix} s_0 & s_1 & s_2 & s_3 & s_4 & s_5 \end{bmatrix}^T = \mathbf{x}\mathbf{s}. \quad (6)$$

According to Fig.1 (a), the evaluation of the nodal displacement vector $\bar{\mathbf{u}}_1^{(e)}$ of the 1D element gives:

$$\bar{\mathbf{u}}_1^{(e)} = \begin{bmatrix} 1 & -d_e & d_e^2 & -d_e^3 & d_e^4 & -d_e^5 \\ 0 & 1 & -2d_e & 3d_e^2 & -4d_e^3 & 5d_e^4 \\ 0 & 0 & 2 & -6d_e & 12d_e^2 & -20d_e^3 \\ 1 & d_e & d_e^2 & d_e^3 & d_e^4 & d_e^5 \\ 0 & 1 & 2d_e & 3d_e^2 & 4d_e^3 & 5d_e^4 \\ 0 & 0 & 2 & 6d_e & 12d_e^2 & 20d_e^3 \end{bmatrix} \mathbf{s} = \mathbf{d}\mathbf{s}. \quad (7)$$

Then, submitting Eq.7 into Eq.6, the displacement vector within the 1D element can be derived by employing the six quintic Hermite polynomial shape function and nodal displacement vector, as follows:

$$U_1 = \mathbf{x}\mathbf{d}^{-1}\bar{\mathbf{u}}_1^{(e)} = \mathbf{N}(x)\bar{\mathbf{u}}_1^{(e)}, \quad (8)$$

in which the shape function $\mathbf{N}(x)$ is expressed in Appendix A.

On the other hand, according to the calculating process above, the shape functions along y and z directions can be expressed as: $\mathbf{N}(y)=\mathbf{N}(x)|_{x=y}=[N_1^0(y), N_1^1(y), N_1^2(y), N_2^0(y), N_2^1(y), N_2^2(y)]$, $\mathbf{N}(z)=\mathbf{N}(x)|_{x=z}=[N_1^0(z), N_1^1(z), N_1^2(z), N_2^0(z), N_2^1(z), N_2^2(z)]$. Then, the shape function of the hexahedral element, as shown in Fig.1 (b), can be developed by expanding the relation of the 1D element to the 3D [58, 59], as follows:

$$\mathbb{N}(x, y, z) = \begin{bmatrix} \mathbf{N}_1(x, y, z) \otimes \mathbf{E}_1 \\ \mathbf{N}_2(x, y, z) \otimes \mathbf{E}_2 \\ \mathbf{N}_3(x, y, z) \otimes \mathbf{E}_3 \end{bmatrix}, \quad (9)$$

in which the element of $\mathbf{N}_p(x, y, z)$ and \mathbf{E}_p ($p = 1, 2, 3$) are defined as:

$$\begin{aligned} N_p^{i(j,k,l)}(x, y, z) &= N_{i'}^j(x)N_{i''}^k(y)N_{i'''}^l(z), \\ \mathbf{E}_p &= \begin{bmatrix} \epsilon_{p1} & \epsilon_{p2} & \epsilon_{p3} \end{bmatrix}, \end{aligned} \quad (10)$$

where $i = 1, \dots, 8$. $j, k, l = 0, 1, 2$. $N_p^{i(j,k,l)}(x, y, z)$ is associated with the DOFs $\partial^{j+k+l}u_i^i/(\partial x^j \partial y^k \partial z^l)$ of node i of the hexahedron element. $i', i'', i''' = 1, 2$ relate to the node number in the corresponding 1D element and they take values of 1 or 2 if the coordinate value of node i is $-d_e$ or d_e . For example, $N_1^{2(1,2,2)}(x, y, z)=N_2^1(x)N_1^2(y)N_1^2(z)$. $\epsilon_{pq} = 1$ for $p = q$. $\epsilon_{pq} = 0$ for $p \neq q$ ($q = 1, 2, 3$).

The displacement vector $\mathbf{U}(x, y, z)$ within the 3D element can be expressed by employing the 3D shape function $\mathbb{N}(x, y, z)$ and the nodal displacement vector $\mathbf{u}^{(e)}$:

$$\mathbf{U}(x, y, z, t) = \mathbb{N}(x, y, z)\mathbf{u}^{(e)}(t), \quad (11)$$

where $\mathbf{u}^{(e)}=[(\mathbf{u}_1^{(e)})^T, (\mathbf{u}_2^{(e)})^T, (\mathbf{u}_3^{(e)})^T]^T$, $(\mathbf{u}_p^{(e)})^T=[(\mathbf{u}_p^{1(e)})^T, (\mathbf{u}_p^{2(e)})^T, \dots, (\mathbf{u}_p^{8(e)})^T]^T$ ($p = 1, 2, 3$). Then, integrating the strain energy density over its volume to obtain the strain potential energy \mathcal{U} as:

$$\mathcal{U} = \int_V \bar{\mathcal{U}} dV = \frac{1}{2} \mathbf{u}^{(e)T} \mathbf{K}^{(e)} \mathbf{u}^{(e)}. \quad (12)$$

On the other hand, the kinetic energy, formed by classical part and non-classical part, is expressed as [60]:

$$\mathcal{T} = \frac{1}{2} \rho \int_{\Omega} \left(\dot{\mathbf{U}} \cdot \dot{\mathbf{U}} + l_1^2 \nabla \dot{\mathbf{U}} : \nabla \dot{\mathbf{U}} + l_2^4 \nabla \nabla \dot{\mathbf{U}} : \nabla \nabla \dot{\mathbf{U}} \right) d\Omega, \quad (13)$$

where ρ denotes the linear mass density, l_1 and l_2 are higher-order length-scale parameters. In our work, the form of kinetic energy is simplified to consider the classical part only [61], whose applications can be found in [62, 63, 64]. There are two main reasons for not considering non-classical part. Firstly, as introduced by Mindlin [27], the mass consists of two parts in micro-structure. The first part comes from macro-material per unit volume which is the majority part. The second part called non-classical part comes from micro-material per unit volume whose proportion is very small. In second strain gradient theory, the main influence on the mechanical properties of the micro-structure comes from the higher-order strain terms in the strain energy density and macro-inertia per unit volume. The influence of micro-inertia appears especially at high frequency [65], whose proportion, however, is secondary compared to macro-inertia and are often omitted [61]. Secondly, the material used in this work is pure metals with the large identical crystal grains. Other micro-materials in the crystal can be considered absent. So, the micro-inertia from micro-material was ignored in this work. As a result:

$$\mathcal{T} = \frac{1}{2} \int_V \left(\frac{\partial \mathbf{U}}{\partial t} \right)^T \rho \left(\frac{\partial \mathbf{U}}{\partial t} \right) dV = \frac{1}{2} \left(\frac{\partial \mathbf{u}^{(e)}}{\partial t} \right)^T \mathbf{M} \left(\frac{\partial \mathbf{u}^{(e)}}{\partial t} \right). \quad (14)$$

Meanwhile, the work done $\delta \mathcal{W}$ by external force can be expressed as:

$$\delta \mathcal{W} = \int_V \delta \mathbf{U}^T \mathbf{f}_V dV + \int_S \delta \mathbf{U}^T \mathbf{f}_S dS = \delta \mathbf{u}^{(e)T} \mathbf{F}^{(e)}, \quad (15)$$

where \mathbf{f}_V is the volume force, \mathbf{f}_S means the face force. By introducing 3D element stiffness and mass matrices and the force vector:

$$\begin{aligned} \mathbf{K}^{(e)} &= \int_V \left(\mathbf{N}^T \boldsymbol{\Psi}_1^T \mathbf{L} \boldsymbol{\Psi}_1 \mathbf{N} + \mathbf{N}^T \boldsymbol{\Psi}_2^T \mathbf{A} \boldsymbol{\Psi}_2 \mathbf{N} + \mathbf{N}^T \boldsymbol{\Psi}_3^T \mathbf{B} \boldsymbol{\Psi}_3 \mathbf{N} + 2 \mathbf{N}^T \boldsymbol{\Psi}_3^T \mathbf{C} \boldsymbol{\Psi}_1 \mathbf{N} \right) dV, \\ \mathbf{M}^{(e)} &= \int_V \left(\mathbf{N}^T \rho \mathbf{N} \right) dV, \\ \mathbf{F}^{(e)} &= \int_V \left(\mathbf{N}^T \mathbf{f}_V \right) dV + \int_S \left(\mathbf{N}^T \mathbf{f}_S \right) dS, \end{aligned} \quad (16)$$

the Hamilton's principle in time domain leads to:

$$\int_{t_1}^{t_2} (\delta \mathcal{U} - \delta \mathcal{W} - \delta \mathcal{T}) dt = \int_{t_1}^{t_2} \left[\delta \mathbf{u}^{(e)T} \left(\mathbf{M}^{(e)} \frac{\partial^2 \mathbf{u}^{(e)}}{\partial t^2} + \mathbf{K}^{(e)} \mathbf{u}^{(e)} - \mathbf{F}^{(e)} \right) \right] dt = 0. \quad (17)$$

3. Waveguide diffusion modeling by WFEM

This section is concerned with the characterization of coupling conditions between two semi-infinite periodic waveguides which are connected through an elastic coupling element at surfaces 1 and 2 as shown in Fig.2(a). Here, it should be noted that the coupling element is only subject to the coupling actions, which means there is no external force applied inside the element. The reflection coefficients (\mathbf{R}) and transmission coefficients (\mathbf{T}) are introduced through simple coupling condition and complex coupling condition respectively as explained in Sec.1.

In order to analyse the wave diffusion characteristics, firstly, the wave propagation of the periodic structure should be investigated through the spectral analysis of a unit cell [49]. Our study focuses on the description of wave propagation along x direction in a slender waveguide, as shown in Fig.2(b), which is composed of identical unit cells coupled together. The dynamics of the system is formulated by using WFEM which offers a numerical wave characterization of periodic structures. The governing equation for a unit cell of length d_1 can be written as:

$$\mathbf{K} \mathbf{u}(t) + \mathbf{C} \frac{\partial \mathbf{u}(t)}{\partial t} + \mathbf{M} \frac{\partial^2 \mathbf{u}(t)}{\partial t^2} = \mathbf{F}, \quad (18)$$

where \mathbf{K} and \mathbf{M} denote the unit cell stiffness and mass matrices assembled using the element stiffness and mass matrices ($\mathbf{K}^{(e)}$, $\mathbf{M}^{(e)}$) defined in the previous section, $\mathbf{C} = \eta \mathbf{K} / \omega$ is defined as damping matrix considering damping lose factor η , \mathbf{u} is nodal displacement vector, \mathbf{F} represents nodal force vector. Assuming that \mathbf{u} and \mathbf{F} are harmonic, the

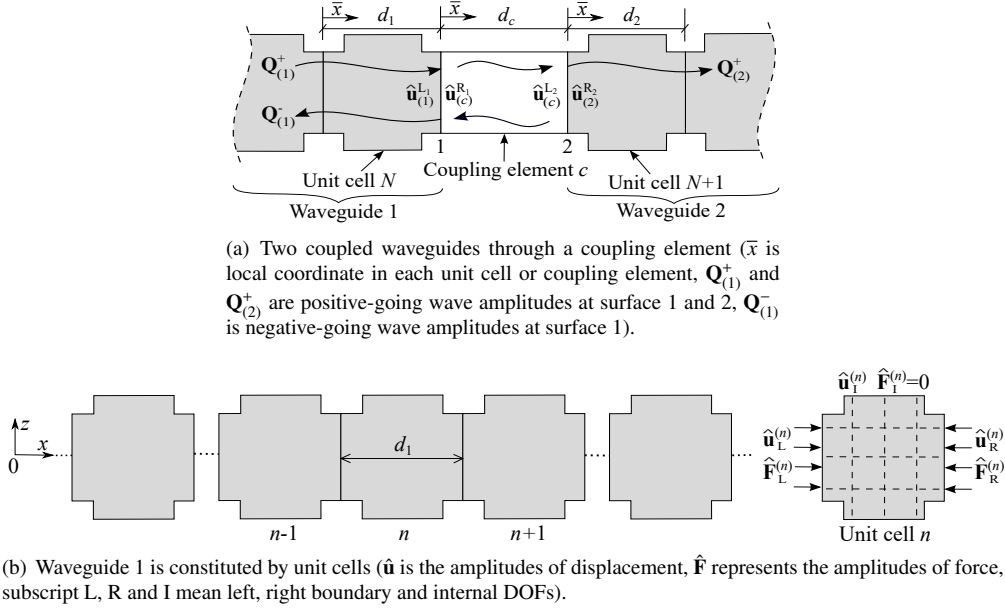


Fig. 2: Two waveguides coupled by a coupling element c and each waveguide is composed of unit cells.

dynamic stiffness matrix will be written as $\mathbf{D}=\mathbf{K}(1+i\eta)-\mathbf{M}\omega^2$ in frequency domain. Then, Eq. 18 can be re-expressed by dividing the DOFs into left boundary (L), internal (I) and right boundary (R) DOFs, as described in Fig. 2(b), this yields:

$$\begin{bmatrix} \mathbf{D}_{LL} & \mathbf{D}_{LI} & \mathbf{D}_{LR} \\ \mathbf{D}_{IL} & \mathbf{D}_{II} & \mathbf{D}_{IR} \\ \mathbf{D}_{RL} & \mathbf{D}_{RI} & \mathbf{D}_{RR} \end{bmatrix} \begin{pmatrix} \hat{\mathbf{u}}_L \\ \hat{\mathbf{u}}_I \\ \hat{\mathbf{u}}_R \end{pmatrix} = \begin{pmatrix} \hat{\mathbf{F}}_L \\ \hat{\mathbf{F}}_I \\ \hat{\mathbf{F}}_R \end{pmatrix}, \quad (19)$$

in which $\hat{\mathbf{u}}$ and $\hat{\mathbf{F}}$ are the amplitudes of \mathbf{u} and \mathbf{F} , respectively. Assuming that the force acts on the left and right boundaries only [47], which means $\hat{\mathbf{F}}_I = 0$. The dynamic equilibrium equation will be re-written as:

$$\begin{bmatrix} \mathbb{D}_{LL} & \mathbb{D}_{LR} \\ \mathbb{D}_{RL} & \mathbb{D}_{RR} \end{bmatrix} \begin{pmatrix} \hat{\mathbf{u}}_L \\ \hat{\mathbf{u}}_R \end{pmatrix} = \begin{pmatrix} \hat{\mathbf{F}}_L \\ \hat{\mathbf{F}}_R \end{pmatrix}, \quad (20)$$

where $\mathbb{D}=\mathbf{D}_{BB}-\mathbf{D}_{BI}\mathbf{D}_{II}^{-1}\mathbf{D}_{IB}$ is the condensed form of dynamic stiffness matrix, subscript B represents the DOFs on the unit cell boundaries. Eq. 20 is the expression of the WFEM analysis that relates the displacement and force on the left and right boundaries of unit cell. For the solution of propagation constants Λ and eigenvectors $\Phi_{\mathbf{u}}$, one can solve the direct Bloch formulation [44, 51] as:

$$\left[\mathbb{D}_{RL}(\omega)\Lambda^{-1} + (\mathbb{D}_{RR}(\omega) + \mathbb{D}_{LL}(\omega)) + \mathbb{D}_{LR}(\omega)\Lambda \right] \Phi_{\mathbf{u}} = 0, \quad (21)$$

where $\Lambda=\text{diag}\{\lambda_j\}_{j=1,\dots,2p}$, $\Phi_{\mathbf{u}}=\{\phi_j\}_{j=1,\dots,2p}$ which can be divided into $\Phi_{\mathbf{u}}^+=\{\phi_j^+\}_{j=1,\dots,p}$ and $\Phi_{\mathbf{u}}^-=\{\phi_j^-\}_{j=p+1,\dots,2p}$. Note that the number of waves is different in the SSG and the CT media. In the following, we denote $p=m$ and $p=n$ the number of waves in the SSG and the CT media, respectively. The propagation constants Λ relating the displacements between two consecutive unit cells can be used to define the positive, negative, propagating and evanescent waves. The waves propagate to the positive direction when $|1/\lambda_j| < 1$. The waves propagate to the negative direction when $|\lambda_j| > 1$. Here, λ_j take the form $\lambda_j=\exp(-i\kappa_j d_{(q)})$, where κ_j is the wavenumber, subscript $q=c$ stands for the coupling element, $q=1$ for waveguide 1, $q=2$ for waveguide 2. It should be noted that a similar spectral analysis is conducted for the coupling element and for waveguides 1 and 2.

Next, the reflection coefficients and transmission coefficients can be calculated through a simple coupling element

as explained in introduction. Assuming that the incident waves come from the infinity of waveguide 1 and there is no reflection from the end of waveguide 2. (The initial boundary of waveguide 1 is also non-reflecting). The local dynamic equilibrium can be written using the state vectors expansion on the positive-going wave amplitudes $\mathbf{Q}_{(1)}^+$ at surface 1, $\mathbf{Q}_{(2)}^+$ at surface 2 and negative-going wave amplitudes $\mathbf{Q}_{(1)}^-$ at surface 1, as shown in Fig.2(a). The \mathbf{R} and \mathbf{T} coefficients [54] can be confirmed in the CT framework. Here should be pointed that there is still no investigation on the diffusion by the SSG theory under simple coupling condition. It is of significance to explore the diffusion properties by the SSG theory.

Last, the diffusion analysis by complex coupling condition, interpreted in introduction part, is studied. As shown in Fig.2(a), the coupling element is described by the SSG theory model. The waveguides are built by the CT model. The description of complex coupling condition enriches the wave propagation and diffusion features in complex system at wave transmission and reflection interfaces. The propagation constant can be re-expressed as $\mathbf{v}_{(q)}^\pm = \text{diag} \left\{ \exp(\mp i \kappa_{j,(q)} \bar{x}) \right\}$ ($\bar{x} = 0, d_{(q)}$), where $\kappa_{j,(q)}$ are obtained from Eq. 21. The displacement field on the left side and right side of coupling element (c) and unit cells ($N, N+1$) can be represented by the superposition of the eigenmodes respectively:

$$\begin{aligned}\hat{\mathbf{u}}_{(q)}^+ &= \Phi_{u,(q)}^+ \mathbf{v}_{(q)}^+|_{\bar{x}=0} \mathbf{Q}_{(q)}^+, \\ \hat{\mathbf{u}}_{(q)}^- &= \Phi_{u,(q)}^- \mathbf{v}_{(q)}^-|_{\bar{x}=0} \mathbf{Q}_{(q)}^-, \\ \hat{\mathbf{u}}_{(q)}^+ &= \Phi_{u,(q)}^+ \mathbf{v}_{(q)}^+|_{\bar{x}=d_{(q)}} \mathbf{Q}_{(q)}^+, \\ \hat{\mathbf{u}}_{(q)}^- &= \Phi_{u,(q)}^- \mathbf{v}_{(q)}^-|_{\bar{x}=d_{(q)}} \mathbf{Q}_{(q)}^-, \end{aligned} \quad (22)$$

where symbol $q=c$ for coupling element, $q=1$ for unit cell N , $q=2$ for unit cell $N+1$. Superscript + means positive-going waves, - means negative-going waves. $\bar{x} = 0$ denotes that the waves start to spread on the left side of the coupling element or unit cell, $\bar{x} = d_{(q)}$ indicates that the waves spread to the right side of the coupling element or unit cell. $\mathbf{Q}_{(q)}$ is the amplitudes of wave modes. On the other hand, the force components on the left side and right side of coupling element (c) and unit cells ($N, N+1$) can be expressed respectively as:

$$\begin{aligned}\hat{\mathbf{F}}_{(q)}^+ &= \Phi_{F,(q)}^+ \mathbf{v}_{(q)}^+|_{\bar{x}=0} \mathbf{Q}_{(q)}^+, \\ \hat{\mathbf{F}}_{(q)}^- &= \Phi_{F,(q)}^- \mathbf{v}_{(q)}^-|_{\bar{x}=0} \mathbf{Q}_{(q)}^-, \\ \hat{\mathbf{F}}_{(q)}^+ &= \Phi_{F,(q)}^+ \mathbf{v}_{(q)}^+|_{\bar{x}=d_{(q)}} \mathbf{Q}_{(q)}^+, \\ \hat{\mathbf{F}}_{(q)}^- &= \Phi_{F,(q)}^- \mathbf{v}_{(q)}^-|_{\bar{x}=d_{(q)}} \mathbf{Q}_{(q)}^-, \end{aligned} \quad (23)$$

in which $\Phi_{F,(q)}^\pm = \mathbb{D}_{LL,(q)} \Phi_{u,(q)}^\pm + \mathbb{D}_{LR,(q)} \Phi_{u,(q)}^\pm \text{diag} \left\{ \exp(\mp i \kappa_{j,(q)} d_{(q)}) \right\}$ according to Eq.20, symbol $q=c$ for coupling element, $q=1$ for unit cell N , $q=2$ for unit cell $N+1$. The eigen-solutions will be same when waveguides 1 and 2 have the same cross-section and material.

The state vector on the right side of surface 1, represented by R_1 , is expressed as:

$$\begin{pmatrix} \hat{\mathbf{u}}_{(c)}^{R_1} \\ \hat{\mathbf{F}}_{(c)}^{R_1} \end{pmatrix} = \begin{bmatrix} \hat{\mathbf{u}}_{(c)}^{R_1+} + \hat{\mathbf{u}}_{(c)}^{R_1-} \\ \hat{\mathbf{F}}_{(c)}^{R_1+} + \hat{\mathbf{F}}_{(c)}^{R_1-} \end{bmatrix} = \begin{bmatrix} \Phi_{u,(c)}^+ & \Phi_{u,(c)}^- \\ \Phi_{F,(c)}^+ & \Phi_{F,(c)}^- \end{bmatrix} \begin{pmatrix} \mathbf{Q}_{(c)}^+ \\ \mathbf{Q}_{(c)}^- \end{pmatrix}, \quad (24)$$

where subscript (c) means coupling element. $\hat{\mathbf{u}}_{(c)}^{R_1+}$ is the positive-going displacement field related to the positive-going waves. $\hat{\mathbf{u}}_{(c)}^{R_1-}$ denotes the negative-going displacement field related to the negative-going waves. $\hat{\mathbf{u}}_{(c)}^{R_1} = \hat{\mathbf{u}}_{(c)}^{R_1+} + \hat{\mathbf{u}}_{(c)}^{R_1-}$ represents the superimposed displacement field on a interface. In addition, the state vector on the left side of surface 2, represented by L_2 , is written as:

$$\begin{pmatrix} \hat{\mathbf{u}}_{(c)}^{L_2} \\ \hat{\mathbf{F}}_{(c)}^{L_2} \end{pmatrix} = \begin{bmatrix} \hat{\mathbf{u}}_{(c)}^{L_2+} + \hat{\mathbf{u}}_{(c)}^{L_2-} \\ \hat{\mathbf{F}}_{(c)}^{L_2+} + \hat{\mathbf{F}}_{(c)}^{L_2-} \end{bmatrix} = \begin{bmatrix} \Phi_{u,(c)}^+ & \Phi_{u,(c)}^- \\ \Phi_{F,(c)}^+ & \Phi_{F,(c)}^- \end{bmatrix} \begin{bmatrix} \mathbf{v}_{(c)}^+|_{\bar{x}=d_c} & \mathbf{0} \\ \mathbf{0} & \mathbf{v}_{(c)}^-|_{\bar{x}=d_c} \end{bmatrix} \begin{pmatrix} \mathbf{Q}_{(c)}^+ \\ \mathbf{Q}_{(c)}^- \end{pmatrix}. \quad (25)$$

Combining Eq.24 and Eq.25, the relation between state vector on left and right side of coupling element will be

conformed:

$$\begin{pmatrix} \hat{\mathbf{u}}_{(c)}^{L_2} \\ \hat{\mathbf{f}}_{(c)}^{L_2} \end{pmatrix} = \mathbf{S}_{(c)} \begin{pmatrix} \hat{\mathbf{u}}_{(c)}^{R_1} \\ \hat{\mathbf{f}}_{(c)}^{R_1} \end{pmatrix}, \quad (26)$$

with

$$\mathbf{S}_{(c)} = \begin{bmatrix} \Phi_{u,(c)}^+ & \Phi_{u,(c)}^- \\ \Phi_{F,(c)}^+ & \Phi_{F,(c)}^- \end{bmatrix} \begin{bmatrix} \mathbf{v}_{(c)}^+|_{\bar{x}=d_c} & \mathbf{0} \\ \mathbf{0} & \mathbf{v}_{(c)}^-|_{\bar{x}=d_c} \end{bmatrix} \begin{bmatrix} \Phi_{u,(c)}^+ & \Phi_{u,(c)}^- \\ \Phi_{F,(c)}^+ & \Phi_{F,(c)}^- \end{bmatrix}^{-1}. \quad (27)$$

Assuming that the incident waves come from the infinity of waveguide 1 and there is no reflection from the end of waveguide 2. The initial boundary of waveguide 1 is also non-reflecting. The state vector on the left side of surface 1, represented by L_1 , is expressed as:

$$\begin{pmatrix} \hat{\mathbf{u}}_{(1)}^{L_1} \\ \hat{\mathbf{f}}_{(1)}^{L_1} \end{pmatrix} = \begin{bmatrix} \hat{\mathbf{u}}_{(1)}^{L_1+} + \hat{\mathbf{u}}_{(1)}^{L_1-} \\ \hat{\mathbf{f}}_{(1)}^{L_1+} + \hat{\mathbf{f}}_{(1)}^{L_1-} \end{bmatrix} = \begin{bmatrix} \Phi_{u,(1)}^+ & \Phi_{u,(1)}^- \\ \Phi_{F,(1)}^+ & \Phi_{F,(1)}^- \end{bmatrix} \begin{bmatrix} \mathbf{v}_{(1)}^+|_{\bar{x}=d_1} \mathbf{Q}_{(1)}^+ \\ \mathbf{v}_{(1)}^-|_{\bar{x}=d_1} \mathbf{Q}_{(1)}^- \end{bmatrix}, \quad (28)$$

in which subscript (1) denotes unit cell N in waveguide 1. The state vector on the right side of surface 2, represented by R_2 , is written as:

$$\begin{pmatrix} \hat{\mathbf{u}}_{(2)}^{R_2} \\ \hat{\mathbf{f}}_{(2)}^{R_2} \end{pmatrix} = \begin{pmatrix} \hat{\mathbf{u}}_{(2)}^{R_2+} \\ \hat{\mathbf{f}}_{(2)}^{R_2+} \end{pmatrix} = \begin{bmatrix} \Phi_{u,(2)}^+ \mathbf{v}_{(2)}^+|_{\bar{x}=0} \mathbf{Q}_{(2)}^+ \\ \Phi_{F,(2)}^+ \mathbf{v}_{(2)}^+|_{\bar{x}=0} \mathbf{Q}_{(2)}^+ \end{bmatrix}, \quad (29)$$

where subscript (2) means unit cell $N + 1$ in waveguide 2. Here should be noted that the size of state vector for coupling element is $2m \times 1$, but $2n \times 1$ for unit cells N and $N+1$. The higher order parts in state vector for coupling element is $2(m - n) \times 1$. In order to ensure the continuity on surfaces 1 and 2, defining new state vectors including higher order parts $(2(m - n) \times 1)$ for unit cells N and $N+1$:

$$\begin{pmatrix} \hat{\mathbf{u}}_{(1)}^{*L_1} \\ \hat{\mathbf{f}}_{(1)}^{*L_1} \end{pmatrix} = \begin{pmatrix} \hat{\mathbf{u}}_{(1)}^{L_1} \\ \hat{\mathbf{f}}_{(1)}^{L_1} \end{pmatrix}, \quad \begin{pmatrix} \hat{\mathbf{u}}_{(2)}^{*R_2} \\ \hat{\mathbf{f}}_{(2)}^{*R_2} \end{pmatrix} = \begin{pmatrix} \hat{\mathbf{u}}_{(2)}^{R_2} \\ \hat{\mathbf{f}}_{(2)}^{R_2} \end{pmatrix}, \quad (30)$$

where $\hat{\mathbf{u}}_{(1)}^{*L_1}$, $\hat{\mathbf{f}}_{(1)}^{*L_1}$ are unknown higher order displacements and forces vectors for unit cell N . $\hat{\mathbf{u}}_{(2)}^{*R_2}$, $\hat{\mathbf{f}}_{(2)}^{*R_2}$ are unknown higher order displacements and forces vectors for unit cell $N+1$. The continuity on surfaces 1 and 2 is:

$$\begin{pmatrix} \hat{\mathbf{u}}_{(c)}^{R_1} \\ \hat{\mathbf{f}}_{(c)}^{R_1} \end{pmatrix} = \begin{pmatrix} \hat{\mathbf{u}}_{(1)}^{*L_1} \\ \hat{\mathbf{f}}_{(1)}^{*L_1} \end{pmatrix}, \quad \begin{pmatrix} \hat{\mathbf{u}}_{(c)}^{L_2} \\ \hat{\mathbf{f}}_{(c)}^{L_2} \end{pmatrix} = \begin{pmatrix} \hat{\mathbf{u}}_{(2)}^{*R_2} \\ \hat{\mathbf{f}}_{(2)}^{*R_2} \end{pmatrix}. \quad (31)$$

Combining Eq.26, Eq.30 and Eq.31, assume that higher order forces vectors for unit cell N and $N+1$ are $\mathbf{0}$. Define $\mathbf{Q}_{(1)}^+ = \mathbf{I}$ as an identity matrix, $\mathbf{Q}_{(1)}^- = \mathbf{R}$, $\mathbf{Q}_{(2)}^+ = \mathbf{T}$, the \mathbf{R} and \mathbf{T} coefficients for complex coupling condition can be conformed as:

$$\begin{bmatrix} \Phi_{u,(2)}^+ \mathbf{v}_{(2)}^+|_{\bar{x}=0} \mathbf{T} \\ \hat{\mathbf{u}}_{(2)}^{R_2} \\ \Phi_{F,(2)}^+ \mathbf{v}_{(2)}^+|_{\bar{x}=0} \mathbf{T} \\ \mathbf{0} \end{bmatrix} = \mathbf{S}_{(c)} \begin{bmatrix} \Phi_{u,(1)}^+ \mathbf{v}_{(1)}^+|_{\bar{x}=d_1} \mathbf{I} + \Phi_{u,(1)}^- \mathbf{v}_{(1)}^-|_{\bar{x}=d_1} \mathbf{R} \\ \hat{\mathbf{u}}_{(1)}^{L_1} \\ \Phi_{F,(1)}^+ \mathbf{v}_{(1)}^+|_{\bar{x}=d_1} \mathbf{I} + \Phi_{F,(1)}^- \mathbf{v}_{(1)}^-|_{\bar{x}=d_1} \mathbf{R} \\ \mathbf{0} \end{bmatrix}. \quad (32)$$

4. Numerical applications

In this part, the WFEM is applied to analyze the multi-mode propagation and diffusion. Materials Aluminum (Al) and Copper (Cu) are used. As shown in Fig.3, $d_y = d_z = 300a_{0(\text{Al})}$ for Al, $d_y = d_z = 337.448a_{0(\text{Cu})}$ for Cu, $d_{1/2} = 50a_{0(\text{Al})}$. For the simple coupling condition: $d_c = 25a_{0(\text{Al})}$ for Al, $d_c = 28.121a_{0(\text{Cu})}$ for Cu. For the complex coupling condition: $d_c = 100a_{0(\text{Al})}$ for Al, $d_c = 112.483a_{0(\text{Cu})}$ for Cu. The lattice parameter $a_{0(\text{Al})} = 4.046 \times 10^{-10}$ m for Al, $a_{0(\text{Cu})} = 3.597 \times 10^{-10}$ m for Cu [57]. The Young's modulus E is 70 GPa for Al and 110 GPa for Cu, linear mass density ρ is 2.7 g/cm³ for Al and 8.96 g/cm³ for Cu. The damping loss factor $\eta = 1e^{-4}$. Unit cells N and $N+1$

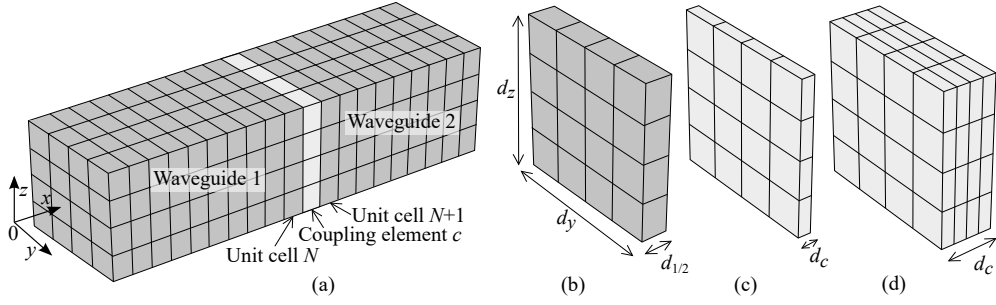


Fig. 3: Finite element model of two waveguides coupled by a coupling element. (b) unit cells N or $N + 1$. (c) a simple coupling element whose modeling is based on the same theory as waveguides. (d) a complex coupling element whose modeling is based on the SSG theory. $d_{1/2}$ are the length along x of unit N or $N + 1$, d_c is the length along x of coupling element, d_y is the length along y and d_z is the length along z .

are meshed into 16 3D elements respectively, coupling element for simple coupling condition is meshed into 16 3D elements but 64 3D elements for complex coupling condition. The higher order parameters for Al and Cu [34] are shown in Tab. 1 and Tab. 2.

Table 1: Higher order material parameters a_i ($eV/\text{\AA}$), c_i ($eV/\text{\AA}$).

Material	a_1	a_2	a_3	a_4	a_5	c_1	c_2	c_3
Al	0.1407	0.0027	-0.0083	0.0966	0.2584	0.5041	0.3569	0.1782
Cu	0.1833	0.0103	0.0010	0.0717	0.1891	0.8448	0.5732	0.3465

Table 2: Higher order material parameters b_i ($eV \cdot \text{\AA}$).

Material	b_1	b_2	b_3	b_4	b_5	b_6	b_7
Al	0.7927	0.0644	-0.1943	-0.0009	0.0009	16.1566	48.5291
Cu	0.6612	0.0663	0.2062	0.0015	0.0015	12.6254	37.9402

4.1. Dispersion relation

The dispersion relation of unit cell N is calculated by WFEM as shown in Fig.4. The real part $\Re(\kappa_j)$ of wavenumber is the phase shift per unit length and the imaginary part $\Im(\kappa_j)$ means the attenuation per unit length. Only the positive waves with real and imaginary parts are illustrated due to the wavenumbers of the negative waves and positive waves are symmetric with respect to x -axis. The frequency is normalized as ω/ω_0 , in which ω_0 is the first nature frequency of the unit cell. The blue lines represent the results from the SSG theory and black lines denote the CT. The curve by the SSG is close to the one by the CT at low frequency. But the difference between the SSG and the CT becomes more obvious as frequency increases. On the other hand, the value of wavenumber κ by the SSG is smaller than the CT at same frequency, especially for bending, tension and torsion modes. This phenomenon can be explained as: the potential energy density in the SSG theory is a function of strain, first gradient of strain and second gradient of strain, which leads to the dynamical equilibrium equation being a high order partial differential function composed of classical part and non-classical part. Due to the existence of non-classical parts containing higher-order parameters, the interactions between microscopic particles within the structure are non-local or long-range, which hardened the stiffness of the material and caused the wavenumber value to decrease. This phenomena clearly demonstrates the effect of size on the structural properties.

In order to verify the WFEM results, the analytical methods referring to the tension, torsion and Timoshenko bending vibration [51, 66, 67] are used. The results from analytical methods match the ones from WFEM, but the difference between them becomes more obvious as frequency increases. Besides the tension, torsion and bending modes, there are high-order modes that analytical methods can not predict. Note that the normalized cut-on frequency for the complex thickness contractional wave 4 [44] is 23 by the CT, instead of 26 by the SSG, and the second-order

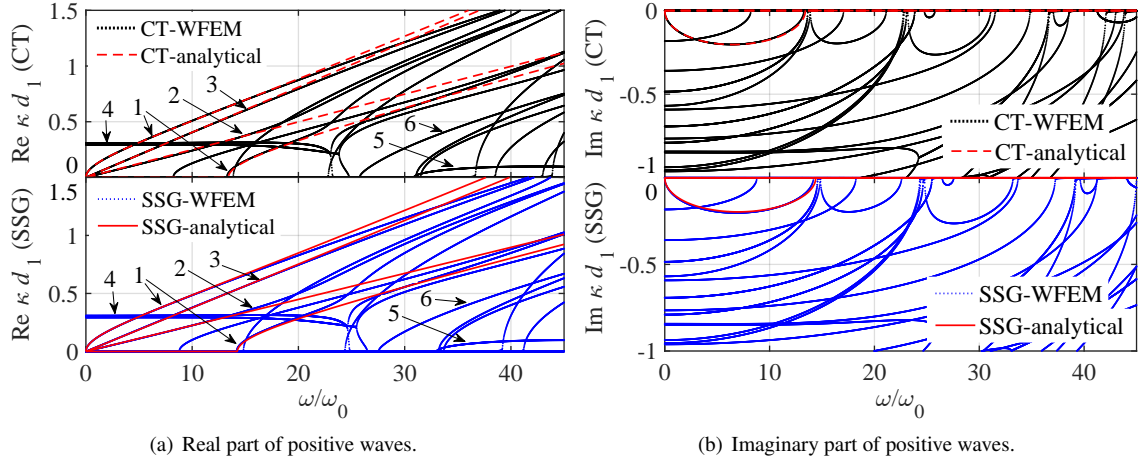


Fig. 4: Dispersion relation of unit cell N (the material is Al) by the SSG and the CT. The horizontal axis is normalized as ω/ω_0 , in which ω_0 is the first nature circular frequency of the unit cell. Besides 1 (bending), 2 (tension) and 3 (torsion) waves, there exist higher order waves. 4: complex thickness contractional wave. 5 and 6: higher order complex waves.

bending wave cuts-on at 13 by the CT but 15 by the SSG. Other waves such as 5 and 6 are more complex, which lead to confusions in the wave modes classification.

Here, the aliasing effects should be introduced. The practical implementation of the proposed method arises two main problems. The first one is choice of unit cell's size whose value cannot be arbitrary. The second one is the frequency range under consideration. Along the propagation direction, the chosen FE must represent a part of propagating wave along the propagation axis correctly. So, based on Shannon space theorem, pertinent wavelengths or wavenumbers κ_j should be connected to the propagation distance: $\text{Re}(\kappa_j(\omega)) < \pi/d_1$. However, this value is too far removed from practical applications. Practically, wavenumbers prediction should start at around 6 to 10 elements per wavelength. As a result, errors and deviations are expected to appear around $\text{Re}(\kappa_j(\omega)) < \pi/3d_1$ or $\text{Re}(\kappa_j(\omega)) < \pi/6d_1$. Large values of d_1 will limit the wavenumber validity domain, and consequently the given frequency range leading to aliasing. Small values of the propagation distance d_1 will lead to two difficulties. The first one is connected to the nature of employed FE. Depending on cross section shape, d_1 should respect strain and stress intrinsic limitations. The second problem is mainly numerical. Small propagation distances will lead to eigenvalues close to unity.

4.2. Effects of higher order parameters

As mentioned in previous section, the dispersion relations are influenced by the higher-order parameters a_i ($i = 1, \dots, 5$), b_j ($j = 1, \dots, 7$) and c_k ($k = 1, \dots, 3$) in the SSG framework. In order to study the effects of these parameters on the results, each parameter is multiplied by a ratio ($\delta_a a_i, \delta_b b_j, \delta_c c_k$) and the influence of these parameters on the results will be analysed by changing the value of $\delta_a, \delta_b, \delta_c$ as -100, -10, -1, -0.5, 0, 0.5, 1, 10, 100. In this work, four different cases are presented. Case 1: $\delta_a, \delta_b, \delta_c$ change at the same time. Case 2: δ_a changes only. Case 3: δ_b changes only and in case 4: δ_c changes only.

The joint effects of a_i, b_j and c_k on the bending dispersion relations including real part and imaginary part are presented in Fig.5 (a). When $\delta_a = \delta_b = \delta_c = -100$, the value of wavenumber is the largest in real part but smallest in imaginary part. When $\delta_a = \delta_b = \delta_c = 100$, the value of wavenumber is the smallest in real part but largest in imaginary part. What is more, as the ratio increases, the value of the real part decreases but the imaginary value increases. On the other hand, the individual effects of a_i, b_j and c_k on the value of wavenumber are shown in Fig.5 (b), Fig.5 (c) and Fig.5 (d) respectively. Each parameter has an impact on the dispersion curve. It can be clearly seen that the value of the real part decreases but the imaginary value increases as the ratio increases. However, parameters a_i have the biggest impact on the results but parameters c_k have the smallest impact on the results.

In order to specifically discuss the influence of the parameters on the results, a rate of change for wavenumber is defined as: $\Delta\kappa = (\kappa - \kappa_{\text{SSG}})/\kappa_{\text{SSG}} \times 100\%$, in which κ is the value of wavenumber under different parameter ratio, κ_{SSG} is the value of wavenumber by the SSG theory ($\delta_a = \delta_b = \delta_c = 1$). $\Delta\kappa$ is then calculated when normalized

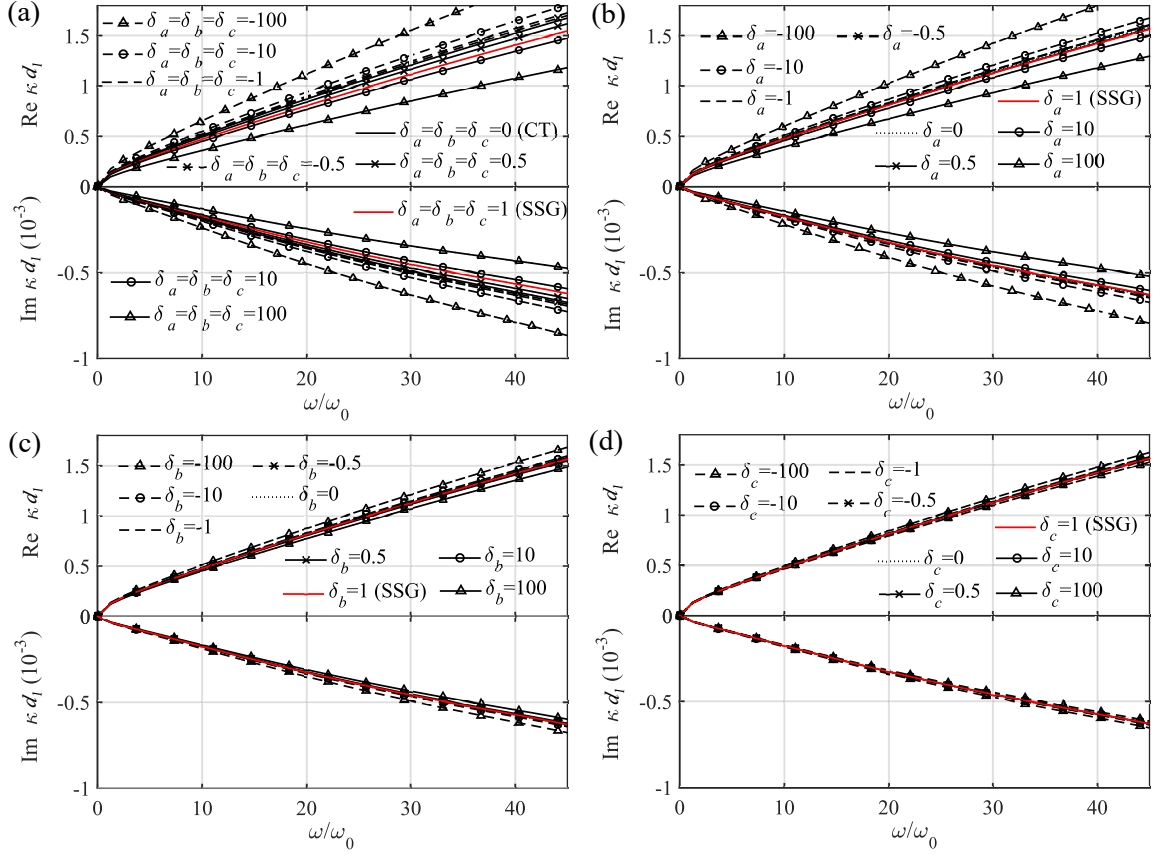


Fig. 5: Effects of higher order parameters for bending including real and imaginary parts of positive waves. (a) case 1: joint effects of a_i, b_j, c_k ($\delta_a, \delta_b, \delta_c$ change as -100, -10, -1, -0.5, 0, 0.5, 1, 10, 100 at the same time). (b) case 2: effects of a_i (δ_a changes as -100, -10, -1, -0.5, 0, 0.5, 1, 10, 100, $\delta_b=\delta_c=1$). (c) case 3: effects of b_j (δ_b changes as -100, -10, -1, -0.5, 0, 0.5, 1, 10, 100, $\delta_a=\delta_c=1$). (d) case 4: effects of c_k (δ_c changes as -100, -10, -1, -0.5, 0, 0.5, 1, 10, 100, $\delta_a=\delta_b=1$).

Table 3: Effects of higher order parameters to real and imaginary part of bending ($\omega/\omega_0=30$).

$\delta_{a b c}$	-100	-10	-1	-0.5	0	0.5	1(SSG)	10	100
$\Delta\kappa(\delta_a, \delta_b, \delta_c)$	35.87	9.69	3.92	3.42	1.94(CT)	0.48	0	-5.24	-23.19
$\Delta\kappa(\delta_a, \delta_b=\delta_c=1)$	24.54	6.63	2.68	2.34	1.33	0.33	0	-3.59	-15.87
$\Delta\kappa(\delta_b, \delta_a=\delta_c=1)$	5.66	1.53	0.62	0.54	0.31	0.08	0	-0.83	-3.66
$\Delta\kappa(\delta_c, \delta_a=\delta_b=1)$	1.89	0.51	0.21	0.18	0.10	0.03	0	-0.28	-1.22

frequency is chosen as 30 under different parameter ratio. As shown in Tab. 3 for bending, with the ratio of parameters increases, the value of $\Delta\kappa$ decreases. At the same ratio of parameter, δ_a, δ_b and δ_c together have a bigger impact on the results than their respective effect on the results. For example, $\Delta\kappa=35.87$ when $\delta_a=\delta_b=\delta_c=-100$; $\Delta\kappa=24.54$ when $\delta_a=-100, \delta_b=\delta_c=1$; $\Delta\kappa=5.66$ when $\delta_b=-100, \delta_a=\delta_c=1$; $\Delta\kappa=1.89$ when $\delta_c=-100, \delta_a=\delta_b=1$. On the other hand, the sum of the value $\Delta\kappa(\delta_a, \delta_b=\delta_c=1)$, $\Delta\kappa(\delta_b, \delta_a=\delta_c=1)$ and $\Delta\kappa(\delta_c, \delta_a=\delta_b=1)$ is approximately equal to the combined value $\Delta\kappa(\delta_a, \delta_b, \delta_c)$. What is more, When $\delta_a = \delta_b = \delta_c=0$, the result belongs to the CT. When $\delta_a = \delta_b = \delta_c=1$, the result belongs to the SSG.

4.3. Diffusion analysis

In this part, firstly, the diffusion is discussed through a simple coupling element as introduced in Sec.1. As shown in Fig.3(c), when the material of coupling element is same as the waveguides, the incident waves will be fully transmitted without reflection. The value of transmission coefficient is 1 and the value of reflection coefficient is

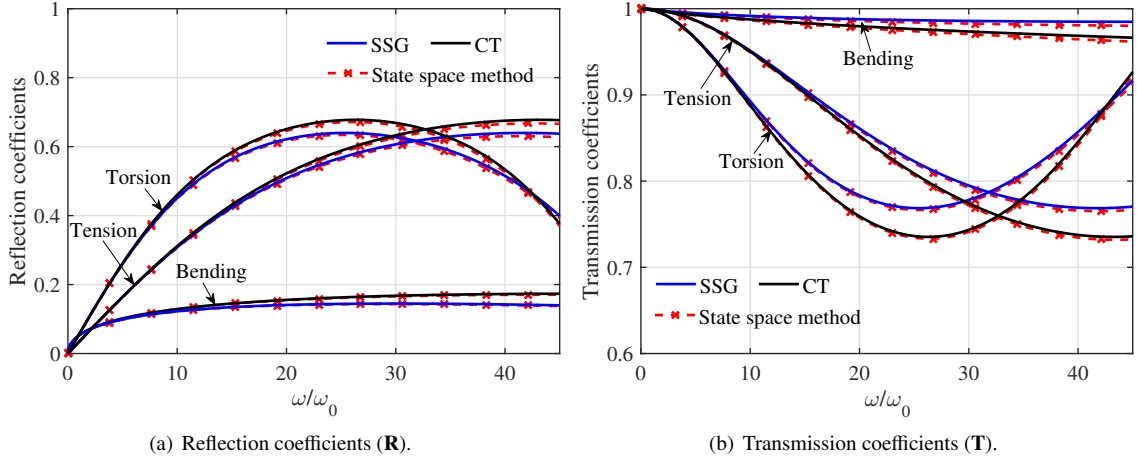


Fig. 6: Absolute values of diffusion coefficients by the SSG and the CT. The horizontal axis is normalized as ω/ω_0 , in which ω_0 is the first nature circular frequency of the unit cell. The material of coupling element is Cu, unit cell N and $N+1$ are Al.

0. When the material of coupling element is Cu and the material of waveguides are Al, there exist wave reflection and transmission. The resulting **R** and **T** coefficients can be illustrated [54]. As shown in Fig.6(a) and Fig.6(b), the diffusion coefficients including bending, tension and torsion modes are presented by the CT and the SSG theory. The blue lines represent the results from the SSG theory and black lines denote the CT. The curve by the SSG is close to the one by the CT at low frequency. The difference between the SSG and the CT becomes more obvious as frequency increases. For bending, tension and torsion modes, the value of reflection coefficient by the CT is bigger than the one by the SSG. However, the value of transmission coefficient by the CT is smaller than the one by the SSG. The difference between the SSG and the CT diffusion coefficients, especially at high frequency, is due to the size effects. The special properties of the micro-structures, such as the stiffness-hardening phenomenon, can be efficiently explored by using the SSG theory. In order to verify the WFEM results, a FE method called the state space method [68], in which the eigenvectors are composed of the displacement part and the force part, is used. The results from two different methods match each other well.

Secondly, in order to study the wave diffusion under a complex coupling condition as explained in Sec.1, as

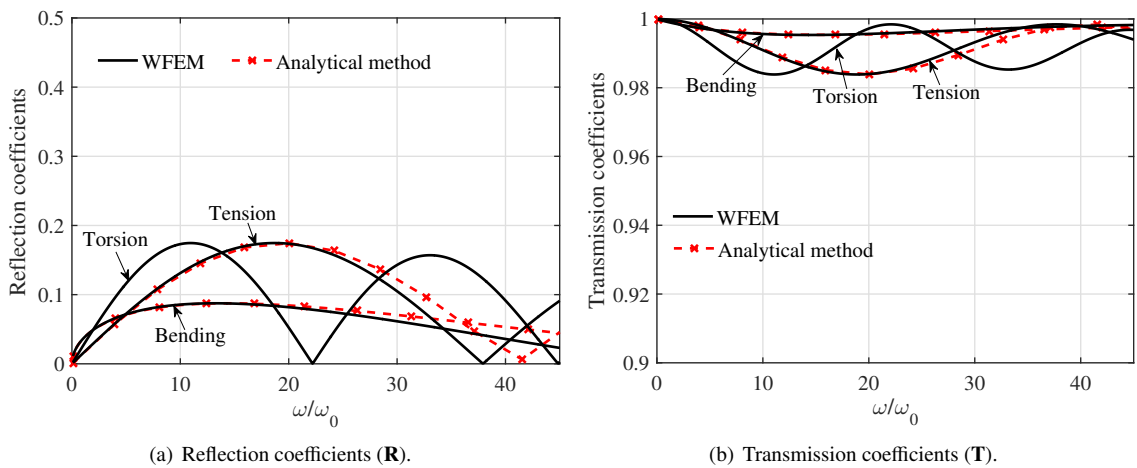


Fig. 7: Absolute values of diffusion coefficients. The horizontal axis is normalized as ω/ω_0 , in which ω_0 is the first nature circular frequency of the unit cell. The materials of coupling element, unit cell N and $N+1$ are Al.

shown in Fig.3(d), defining the the materials of coupling element, unit cell N and $N+1$ are Al, the diffusion model of coupling element is built by the SSG theory with higher-order parameters, the diffusion models of unit cell N and $N+1$ are built by CT. The \mathbf{R} and \mathbf{T} coefficients can be calculated from Eq. 32 including bending, tension and torsion modes. As shown in Fig.7, the black lines denote the WFEM results. The value of \mathbf{R} representing the non-classical part of reflection is no longer 0, and the value of \mathbf{T} representing the non-classical part of transmission is no longer 1. The influence of non-local interactions caused by higher-order parameters can be reflected by this model. On the other hand, an analytical method [38], shown by the red lines, is used to valid the WFEM results for bending and tension. As we can see, for \mathbf{R} , the result obtained by WFEM is very close to the one by the analytical method at low frequency, but the results are different at high frequencies. For \mathbf{T} , the result by WFEM matches the results by analytical method well.

In addition, the joint influence of classical parameters (i. g., Young's modulus, Poisson's ratio and mass density)

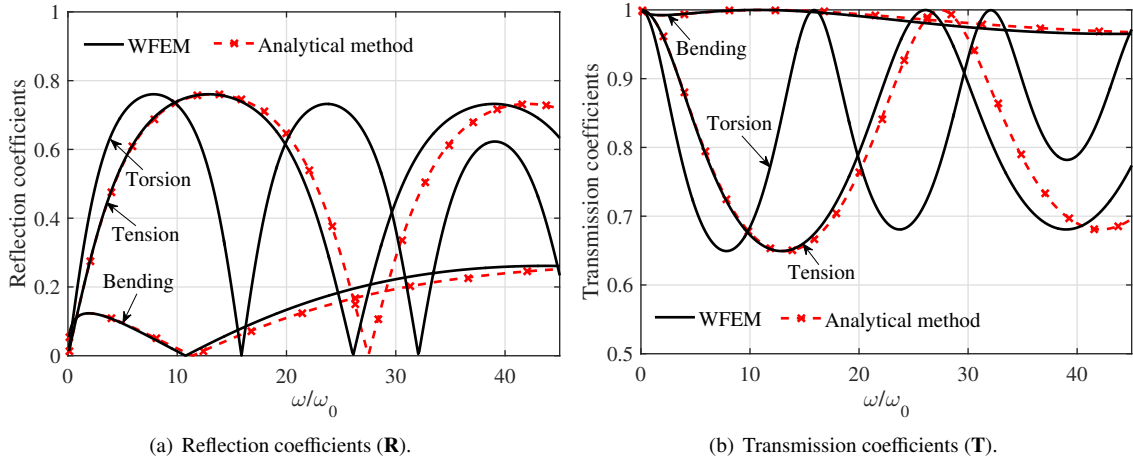


Fig. 8: Absolute values of diffusion coefficients. The horizontal axis is normalized as ω/ω_0 , in which ω_0 is the first nature circular frequency of the unit cell. The material of coupling element is Cu, unit cell N and $N+1$ are Al.

and higher-order parameters of material on diffusion is also a very meaningful study. Defining the material of coupling element is Cu, unit cell N and $N+1$ are Al, the diffusion model of coupling element is built by the SSG theory with higher-order parameters, the diffusion models of unit cell N and $N+1$ are built by CT. The \mathbf{R} and \mathbf{T} coefficients including bending, tension and torsion modes can be illustrated by Eq. 32 as well. As shown in Fig.8, the black lines denote the WFEM results and the red lines represent the results from an analytical method [38]. The diffusion is different from the case presented in Fig.7, this shows that the impedance mismatch is not only due to the non-local interactions caused by higher order parameters in the SSG theory model but also the local interactions caused by classical parameters.

4.4. Forced response

In this part, the forced response for waveguide 1 is discussed, as presented in Fig. 3(a), the waveguide 1 consists of 10 unit cells. There are two boundary conditions in this study: the first one is that left end of waveguide 1 is clamped, right end of waveguide 1 is free (C-F), the second one is that left and right ends of waveguide 1 are free (F-F). A harmonic force with a unit amplitude is loaded at center point of right end along z direction. Then, the amplitude of displacement at center point of right end is calculated out on each frequency according to $\mathbf{D}^*\mathbf{u}^*=\mathbf{F}^*$, in which \mathbf{D}^* is the global dynamical stiffness matrix of waveguide 1 assembled from a unit cell dynamical stiffness matrix \mathbf{D} .

The forced responses for C-F and F-F boundary conditions are shown in Fig. 9(a) and Fig. 9(b) respectively by the SSG theory and the CT. It can be noticed that resonances are well predicted in both theories. The comparison between the SSG theory and the CT shows that at low frequency, the forced response by the SSG confirms to the CT well. On the other hand, same as for the dispersion curves, the discrepancies of forced responses between the CT and the SSG increase with frequency increases. The wave propagation is significantly affected by the long-range

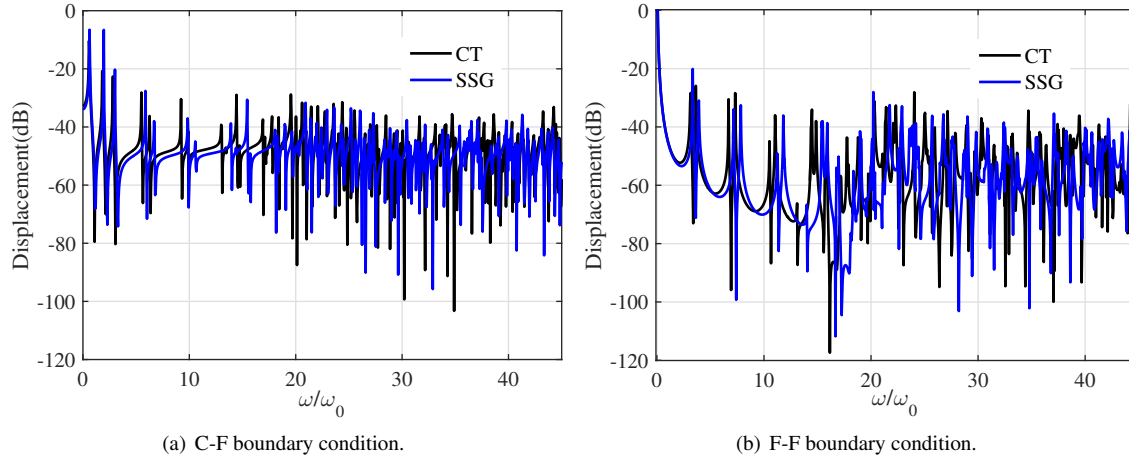


Fig. 9: Forced response of waveguide 1 by the SSG and the CT. The horizontal axis is normalized as ω/ω_0 , in which ω_0 is the first nature circular frequency of the unit cell.

interactions in micro-sized structure caused by the non-classical parts in the SSG theory. The input vibration energy can be transferred both by propagating waves and other evanescent waves, which decay rapidly in the near field of the excitation.

5. Conclusions

In this paper, the Second Strain Gradient (SSG) theory is used for the multi-mode propagation and diffusion analysis within the Wave Finite Element Method (WFEM) framework. In order to explore the dynamical properties of micro-sized 3D beam, firstly, the constitutive relations of 3D micro-sized model are introduced in the SSG theory framework. The displacement vector is derived by employing the six quin-tic Hermite polynomial shape function. The weak formulations including element stiffness, mass matrices and force vector are calculated by using the Hamilton's principle and global dynamic stiffness matrix of a unit cell is assembled.

Subsequently, the dispersion relation for a 3D beam is illustrated by the SSG and the CT. The results show that the existence of non-classical parts containing higher-order parameters in the SSG theory can exert stiffness-hardening mechanisms. The discrepancy between the SSG and the CT appears at high frequency in the dispersion relation, which shows the importance of using the SSG theory to reflect the size effects in the micro-sized structures at high frequency. The κ value by the SSG is smaller than the CT at same frequency, especially for bending, tension and torsion modes. The effects of a_i , b_j and c_k on the bending dispersion relations are presented. The effect of a_i on the result is biggest and the effect of c_i on the result is smallest.

On the other hand, the diffusion is confirmed through three different cases. It is found that for the first case, the diffusion curve by the SSG is close to the one by the CT at low frequency. However, the difference between the SSG and the CT becomes more obvious as frequency increases. For the second case, the value of \mathbf{R} representing the non-classical part of reflection is no longer 0, and the value of \mathbf{T} representing the non-classical part of transmission is no longer 1. The influence of non-local interactions caused by higher-order parameters can be reflected by this model. The third case shows that the impedance mismatch is not only due to the non-local interactions caused by higher order parameters in the SSG theory model but also the local interactions caused by classical parameters such as Young's modulus, Poisson's ratio and mass density.

Last, the forced responses including two boundary conditions for waveguide 1 are discussed. Results obtained show that at low frequency, the forced response curve by the SSG is close to the one by the CT. Same as the dispersion curves, the discrepancies of forced responses between the CT and the SSG increase with frequency increases. Wave propagation is significantly affected by the long-range interactions in micro-sized structure.

Acknowledgements

This work is supported by the LabEx CeLyA (Centre Lyonnais d'Acoustique, ANR-10-LABX-0060) of Université de Lyon. The research of B. Yang is funded by the China Scholarship Council (CSC).

Appendix A. Definitions of $\Psi_1, \Psi_2, \Psi_3, \mathbf{L}, \mathbf{A}, \mathbf{B}, \mathbf{C}, \bar{\mathbf{u}}_1^{(e)}, \mathbf{u}_1^{i(e)}$ and $\mathbf{N}(x)$

The matrices Ψ_1, Ψ_2 and Ψ_3 in Eq.3:

$$\Psi_1 = \begin{bmatrix} \partial_x & 0 & 0 \\ 0 & \partial_y & 0 \\ 0 & 0 & \partial_z \\ 0 & \partial_z & \partial_y \\ \partial_z & 0 & \partial_x \\ 0 & \partial_y & \partial_x \end{bmatrix}, \Psi_2 = \begin{bmatrix} \mathbf{e}_1 & \mathbf{0} & \mathbf{0} \\ \mathbf{0} & \mathbf{e}_1 & \mathbf{0} \\ \mathbf{0} & \mathbf{0} & \mathbf{e}_1 \end{bmatrix} \otimes \begin{bmatrix} \partial_{xx} \\ \partial_{yy} \\ \partial_{zz} \\ 2\partial_{xy} \\ 2\partial_{xz} \\ 2\partial_{yz} \end{bmatrix}, \Psi_3 = \begin{bmatrix} \mathbf{e}_2 & \mathbf{0} & \mathbf{0} \\ \mathbf{0} & \mathbf{e}_2 & \mathbf{0} \\ \mathbf{0} & \mathbf{0} & \mathbf{e}_2 \end{bmatrix} \otimes \begin{bmatrix} \partial_{xxx} \\ \partial_{yyy} \\ \partial_{zzz} \\ 3\partial_{xxy} \\ 3\partial_{xxz} \\ 3\partial_{yyx} \\ 3\partial_{yyz} \\ 3\partial_{zzx} \\ 3\partial_{zzy} \\ 6\partial_{xyz} \end{bmatrix}, \text{ where symbol } \otimes \text{ stands}$$

for the Kronecker product, \mathbf{e}_1 with size 6×1 and \mathbf{e}_2 with size 10×1 are the matrices whose element value is 1.

The matrices $\mathbf{L}, \mathbf{A}, \mathbf{B}$ and \mathbf{C} in Eq.4:

$$\mathbf{L} = \begin{bmatrix} \lambda + 2\mu & \lambda & \lambda & \mathbf{0} \\ \lambda & \lambda + 2\mu & \lambda & \mathbf{0} \\ \lambda & \lambda & \lambda + 2\mu & \mathbf{0} \\ \mathbf{0} & \mathbf{0} & \mathbf{0} & \mu \mathbf{I} \end{bmatrix}, \mathbf{A} = \begin{bmatrix} \mathbf{A}_1 & \mathbf{0} & \mathbf{0} & \mathbf{0} \\ \mathbf{0} & \mathbf{A}_1 & \mathbf{0} & \mathbf{0} \\ \mathbf{0} & \mathbf{0} & \mathbf{A}_1 & \mathbf{0} \\ \mathbf{0} & \mathbf{0} & \mathbf{0} & \mathbf{A}_2 \end{bmatrix},$$

$$\mathbf{B} = \begin{bmatrix} \mathbf{B}_{11} & \mathbf{B}_{12} & \mathbf{B}_{13} & \mathbf{B}_{14} & \mathbf{B}_{15} & \mathbf{B}_{16} \\ \mathbf{B}_{21} & \mathbf{B}_{22} & \mathbf{B}_{23} & \mathbf{B}_{24} & \mathbf{B}_{25} & \mathbf{B}_{26} \\ \mathbf{B}_{31} & \mathbf{B}_{32} & \mathbf{B}_{33} & \mathbf{B}_{34} & \mathbf{B}_{35} & \mathbf{B}_{36} \\ \mathbf{B}_{41} & \mathbf{B}_{42} & \mathbf{B}_{43} & \mathbf{B}_{44} & \mathbf{B}_{45} & \mathbf{B}_{46} \\ \mathbf{B}_{51} & \mathbf{B}_{52} & \mathbf{B}_{53} & \mathbf{B}_{54} & \mathbf{B}_{55} & \mathbf{B}_{56} \\ \mathbf{B}_{61} & \mathbf{B}_{62} & \mathbf{B}_{63} & \mathbf{B}_{64} & \mathbf{B}_{65} & \mathbf{B}_{66} \end{bmatrix}, \mathbf{C} = [\mathbf{C}_1 \quad \mathbf{C}_2 \quad \mathbf{C}_3 \quad \mathbf{C}_4 \quad \mathbf{C}_5 \quad \mathbf{C}_6],$$

$$\text{in which } \mathbf{A}_1 = \begin{bmatrix} \bar{a}_1 & \bar{a}_2 & \bar{a}_2 & \bar{a}_1 & \bar{a}_3 \\ \bar{a}_2 & \bar{a}_4 & 2a_3 & \bar{a}_5 & \frac{a_2}{2} \\ \bar{a}_2 & 2a_2 & \bar{a}_4 & \frac{a_2}{2} & \bar{a}_5 \\ \bar{a}_3 & \bar{a}_5 & \frac{a_2}{2} & \bar{a}_6 & \frac{a_1}{2} \\ \bar{a}_3 & \frac{a_2}{2} & \bar{a}_5 & \frac{a_1}{2} & \bar{a}_6 \end{bmatrix}, \mathbf{A}_2 = \begin{bmatrix} a_4 & \frac{a_5}{2} & \frac{a_5}{2} \\ \frac{a_5}{2} & a_4 & \frac{a_5}{2} \\ \frac{a_5}{2} & \frac{a_5}{2} & a_4 \end{bmatrix}, \mathbf{B}_{11} = \begin{bmatrix} \bar{b}_1 & 0 & 0 & 0 & 0 \\ 0 & \bar{b}_4 & 0 & \bar{b}_7 & 0 \\ 0 & 0 & \bar{b}_4 & 0 & \bar{b}_7 \\ 0 & \bar{b}_7 & 0 & \bar{b}_2 & 0 \\ 0 & 0 & \bar{b}_7 & 0 & \bar{b}_2 \end{bmatrix},$$

$$\mathbf{B}_{12} = \mathbf{B}_{21}^T = \begin{bmatrix} \bar{b}_6 & 0 & \bar{b}_6 & 0 & 0 \\ 0 & 0 & 0 & \frac{2}{3}b_5 & 0 \\ 0 & \frac{2}{3}b_5 & 0 & 0 & 0 \\ 0 & 0 & 0 & \bar{b}_7 & 0 \\ 0 & \frac{\bar{b}_7}{3} & 0 & 0 & 0 \end{bmatrix}, \mathbf{B}_{22} = \begin{bmatrix} \bar{b}_9 + \bar{b}_{11} & 0 & \bar{b}_{11} & 0 & 0 \\ 0 & \bar{b}_5 & 0 & 0 & 0 \\ \bar{b}_{11} & 0 & \bar{b}_9 + \bar{b}_{11} & 0 & 0 \\ 0 & 0 & 0 & \bar{b}_5 & 0 \\ 0 & 0 & 0 & 0 & \frac{\bar{b}_9}{2} \end{bmatrix},$$

$$\mathbf{B}_{33} = \begin{bmatrix} \bar{b}_4 & 0 & 0 & 0 & 0 \\ 0 & \bar{b}_1 & 0 & \frac{\bar{b}_6}{3} & 0 \\ 0 & 0 & \bar{b}_4 & 0 & \frac{2}{3}b_5 \\ 0 & \bar{b}_6 & 0 & \bar{b}_9 + \bar{b}_{11} & 0 \\ 0 & 0 & \frac{2}{3}b_5 & 0 & \bar{b}_5 \end{bmatrix}, \mathbf{B}_{34} = \mathbf{B}_{43}^T = \begin{bmatrix} \bar{b}_7 & 0 & \frac{2}{3}b_5 & 0 & 0 \\ 0 & 0 & 0 & \frac{\bar{b}_6}{3} & 0 \\ 0 & \bar{b}_7 & 0 & 0 & 0 \\ 0 & 0 & 0 & \bar{b}_{11} & 0 \\ 0 & \frac{\bar{b}_7}{3} & 0 & 0 & 0 \end{bmatrix},$$

$$\mathbf{B}_{44} = \begin{bmatrix} \bar{b}_2 & 0 & \frac{\bar{b}_7}{3} & 0 & 0 \\ 0 & \bar{b}_2 & 0 & 0 & 0 \\ \frac{\bar{b}_7}{3} & 0 & \bar{b}_1 & 0 & 0 \\ 0 & 0 & 0 & \bar{b}_9 + \bar{b}_{11} & 0 \\ 0 & 0 & 0 & 0 & \frac{\bar{b}_9}{3} \end{bmatrix}, \mathbf{B}_{55} = \begin{bmatrix} \bar{b}_4 & 0 & 0 & 0 & 0 \\ 0 & \bar{b}_1 & 0 & \frac{2}{3}b_5 & 0 \\ 0 & 0 & \bar{b}_1 & 0 & \bar{b}_6 \\ 0 & \frac{2}{3}b_5 & 0 & \bar{b}_5 & 0 \\ 0 & 0 & \bar{b}_6 & 0 & \bar{b}_9 + \bar{b}_{11} \end{bmatrix},$$

$$\mathbf{B}_{66} = \begin{bmatrix} \bar{b}_5 & 0 & \frac{\bar{b}_7}{3} & 0 & 0 \\ 0 & \bar{b}_9 + \bar{b}_{11} & 0 & 0 & 0 \\ \frac{\bar{b}_7}{3} & 0 & \bar{b}_2 & 0 & 0 \\ 0 & 0 & 0 & \bar{b}_2 & 0 \\ 0 & 0 & 0 & 0 & \frac{\bar{b}_9}{3} \end{bmatrix}, \mathbf{B}_{56} = \mathbf{B}_{65}^T = \begin{bmatrix} \frac{2}{3}b_5 & 0 & \bar{b}_7 & 0 & 0 \\ 0 & 0 & 0 & \bar{b}_7 & 0 \\ 0 & \frac{\bar{b}_6}{3} & 0 & 0 & 0 \\ 0 & 0 & 0 & \frac{\bar{b}_7}{3} & 0 \\ 0 & \bar{b}_{11} & 0 & 0 & 0 \end{bmatrix},$$

$$\mathbf{B}_{13} = \mathbf{B}_{31}^T = \begin{bmatrix} 0 & 2b_1 & 0 & \bar{b}_{13} & 0 \\ 2b_4 & 0 & 0 & 0 & 0 \\ 0 & 0 & 0 & 0 & 0 \\ \bar{b}_{12} & 0 & 0 & 0 & 0 \\ 0 & 0 & 0 & 0 & 0 \end{bmatrix}, \mathbf{B}_{14} = \mathbf{B}_{41}^T = \begin{bmatrix} 0 & 0 & 0 & \frac{2}{3}b_1 & 0 \\ \bar{b}_{12} & 0 & \frac{2}{3}b_4 & 0 & 0 \\ 0 & 0 & 0 & 0 & \frac{b_3}{6} \\ \bar{b}_{10} & 0 & \bar{b}_{17} & 0 & 0 \\ 0 & 0 & 0 & 0 & \bar{b}_{15} \end{bmatrix},$$

$$\mathbf{B}_{23} = \mathbf{B}_{32}^T = \begin{bmatrix} 0 & \bar{b}_{13} & 0 & \bar{b}_3 & 0 \\ 0 & 0 & 0 & 0 & 0 \\ 0 & \frac{2}{3}b_1 & 0 & \bar{b}_{16} & 0 \\ \frac{2}{3}b_4 & 0 & 0 & 0 & 0 \\ 0 & 0 & \frac{b_3}{6} & 0 & \bar{b}_{18} \end{bmatrix}, \mathbf{B}_{24} = \mathbf{B}_{42}^T = \begin{bmatrix} 0 & 0 & 0 & \bar{b}_{16} & 0 \\ 0 & 0 & 0 & 0 & \bar{b}_{18} \\ 0 & 0 & 0 & \bar{b}_{19} & 0 \\ \bar{b}_{17} & 0 & \bar{b}_{14} & 0 & 0 \\ 0 & \bar{b}_{15} & 0 & 0 & 0 \end{bmatrix},$$

$$\mathbf{B}_{15} = \mathbf{B}_{51}^T = \begin{bmatrix} 0 & 0 & 2b_1 & 0 & \bar{b}_{13} \\ 0 & 0 & 0 & 0 & 0 \\ 2b_4 & 0 & 0 & 0 & 0 \\ 0 & 0 & 0 & 0 & 0 \\ \bar{b}_{12} & 0 & 0 & 0 & 0 \end{bmatrix}, \mathbf{B}_{16} = \mathbf{B}_{61}^T = \begin{bmatrix} 0 & \frac{2}{3}b_1 & 0 & 0 & 0 \\ 0 & 0 & 0 & 0 & \frac{b_3}{6} \\ \frac{2}{3}b_4 & 0 & \bar{b}_{12} & 0 & 0 \\ 0 & 0 & 0 & 0 & \bar{b}_{15} \\ \bar{b}_{17} & 0 & \bar{b}_{10} & 0 & 0 \end{bmatrix},$$

$$\mathbf{B}_{25} = \mathbf{B}_{52}^T = \begin{bmatrix} 0 & 0 & \frac{2}{3}b_1 & 0 & \bar{b}_{16} \\ \frac{2}{3}b_4 & 0 & 0 & 0 & 0 \\ 0 & 0 & \bar{b}_{13} & 0 & \bar{b}_3 \\ 0 & 0 & 0 & 0 & 0 \\ 0 & \frac{b_3}{6} & 0 & \bar{b}_{18} & 0 \end{bmatrix}, \mathbf{B}_{26} = \mathbf{B}_{62}^T = \begin{bmatrix} 0 & \bar{b}_{19} & 0 & 0 & 0 \\ \bar{b}_{14} & 0 & \bar{b}_{17} & 0 & 0 \\ 0 & \bar{b}_{16} & 0 & 0 & 0 \\ 0 & 0 & 0 & 0 & \bar{b}_{18} \\ 0 & 0 & 0 & \bar{b}_{15} & 0 \end{bmatrix},$$

$$\mathbf{B}_{35} = \mathbf{B}_{53}^T = \begin{bmatrix} 0 & 0 & 0 & 0 & 0 \\ 0 & 0 & 2b_1 & 0 & \frac{2}{3}b_1 \\ 0 & 2b_4 & 0 & \frac{2}{3}b_4 & 0 \\ 0 & 0 & \frac{4}{3}b_1 & 0 & \bar{b}_{19} \\ 0 & \frac{2}{3}b_4 & 0 & \bar{b}_{14} & 0 \end{bmatrix}, \mathbf{B}_{36} = \mathbf{B}_{63}^T = \begin{bmatrix} 0 & 0 & 0 & 0 & \frac{b_3}{6} \\ 0 & \bar{b}_{13} & 0 & 0 & 0 \\ 0 & 0 & 0 & \bar{b}_{12} & 0 \\ 0 & \bar{b}_{16} & 0 & 0 & 0 \\ 0 & 0 & 0 & \bar{b}_{17} & 0 \end{bmatrix},$$

$$\mathbf{B}_{45} = \mathbf{B}_{54}^T = \begin{bmatrix} 0 & 0 & 0 & 0 & 0 \\ 0 & \bar{b}_{12} & 0 & \bar{b}_{17} & 0 \\ 0 & 0 & 0 & 0 & 0 \\ 0 & 0 & \bar{b}_{13} & 0 & \bar{b}_{16} \\ \frac{b_3}{6} & 0 & 0 & 0 & 0 \end{bmatrix}, \mathbf{B}_{46} = \mathbf{B}_{64}^T = \begin{bmatrix} 0 & 0 & 0 & 0 & \bar{b}_{15} \\ 0 & 0 & 0 & \bar{b}_{10} & 0 \\ 0 & 0 & 0 & 0 & \bar{b}_{18} \\ 0 & \bar{b}_3 & 0 & 0 & 0 \\ \bar{b}_{18} & 0 & \bar{b}_{15} & 0 & 0 \end{bmatrix},$$

$$\mathbf{C}_1 = \begin{bmatrix} \bar{c}_1 & 0 & 0 & 0 & 0 \\ c_1 & 0 & 0 & 0 & 0 \\ c_1 & 0 & 0 & 0 & 0 \\ 0 & 0 & 0 & 0 & 0 \\ 0 & 0 & \frac{c_3}{2} & 0 & \bar{c}_3 \\ 0 & \frac{c_3}{2} & 0 & \bar{c}_3 & 0 \end{bmatrix}, \mathbf{C}_2 = \begin{bmatrix} \bar{c}_2 & 0 & \bar{c}_2 & 0 & 0 \\ \bar{c}_2 & 0 & c_1 & 0 & 0 \\ c_1 & 0 & \bar{c}_2 & 0 & 0 \\ 0 & 0 & 0 & 0 & \frac{c_2}{6} \\ 0 & \frac{c_3}{2} & 0 & 0 & 0 \\ 0 & 0 & 0 & \frac{c_3}{2} & 0 \end{bmatrix}, \mathbf{C}_3 = \begin{bmatrix} 0 & c_1 & 0 & \bar{c}_4 & 0 \\ 0 & \bar{c}_1 & 0 & \bar{c}_2 & 0 \\ 0 & c_1 & 0 & c_1 & 0 \\ 0 & 0 & \frac{c_3}{2} & 0 & \frac{c_3}{2} \\ 0 & 0 & 0 & 0 & 0 \\ \frac{c_3}{2} & 0 & 0 & 0 & 0 \end{bmatrix},$$

$$\mathbf{C}_4 = \begin{bmatrix} 0 & 0 & 0 & c_1 & 0 \\ 0 & 0 & 0 & \bar{c}_2 & 0 \\ 0 & 0 & 0 & \bar{c}_2 & 0 \\ 0 & \bar{c}_3 & 0 & 0 & 0 \\ 0 & 0 & 0 & 0 & \frac{c_2}{6} \\ 0 & 0 & \frac{c_3}{2} & 0 & 0 \end{bmatrix}, \mathbf{C}_5 = \begin{bmatrix} 0 & 0 & c_1 & 0 & \bar{c}_4 \\ 0 & 0 & c_1 & 0 & c_1 \\ 0 & 0 & \bar{c}_1 & 0 & \bar{c}_2 \\ 0 & \frac{c_3}{2} & 0 & \frac{c_3}{2} & 0 \\ \frac{c_3}{2} & 0 & 0 & 0 & 0 \\ 0 & 0 & 0 & 0 & 0 \end{bmatrix}, \mathbf{C}_6 = \begin{bmatrix} 0 & c_1 & 0 & 0 & 0 \\ 0 & \bar{c}_4 & 0 & 0 & 0 \\ 0 & \bar{c}_4 & 0 & 0 & 0 \\ 0 & 0 & 0 & \bar{c}_3 & 0 \\ \frac{c_3}{2} & 0 & \bar{c}_3 & 0 & 0 \\ 0 & 0 & 0 & 0 & \frac{c_2}{6} \end{bmatrix},$$

where $\bar{a}_1=2(a_1 + a_2 + a_3 + a_4 + a_5)$, $\bar{a}_2=a_2 + 2a_3$, $\bar{a}_3=\frac{2a_1 + a_2}{2}$, $\bar{a}_4=2(a_3 + a_4)$, $\bar{a}_5=\frac{a_2 + 2a_5}{2}$, $\bar{a}_6=\frac{a_1 + 2a_4 + a_5}{2}$,
 $\bar{b}_1=2(b_1 + b_2 + b_3 + b_4 + b_5 + b_6 + b_7)$, $\bar{b}_2=\frac{2}{9}(2b_2 + b_3 + b_5 + 3b_6 + 2b_7)$, $\bar{b}_3=\frac{2}{9}(b_1 + b_3 + 2b_7)$, $\bar{b}_4=2(b_5 + b_6)$,
 $\bar{b}_5=\frac{2}{9}(b_5 + 3b_6)$, $\bar{b}_6=(2b_1 + b_3 + 2b_4 + 2b_5)/3$, $\bar{b}_7=\frac{b_3 + 2b_5}{3}$, $\bar{b}_8=\frac{2}{3}(b_1 + b_2 + b_3 + b_4 + b_5)$, $\bar{b}_9=\frac{2}{9}(b_2 + 3b_6 + b_7)$,
 $\bar{b}_{10}=\frac{2}{9}(2b_2 + b_3 + b_4)$, $\bar{b}_{11}=\frac{2}{9}(b_1 + b_4 + b_5)$, $\bar{b}_{12}=\frac{b_3 + 2b_4 + 2b_7}{3}$, $\bar{b}_{13}=\frac{2b_1 + 2b_2 + b_3}{3}$, $\bar{b}_{14}=\frac{2}{9}(b_4 + b_7)$, $\bar{b}_{15}=\frac{4b_2 + b_3}{18}$,
 $\bar{b}_{16}=\frac{2b_1 + b_3}{9}$, $\bar{b}_{17}=\frac{b_3 + 2b_4}{9}$, $\bar{b}_{18}=\frac{b_3 + 4b_7}{18}$, $\bar{b}_{19}=\frac{2}{9}(b_1 + b_2)$, $\bar{c}_1=c_1 + c_2 + c_3$, $\bar{c}_2=\frac{c_1 + c_3}{3}$, $\bar{c}_3=\frac{2c_2 + c_3}{6}$, $\bar{c}_4=\frac{c_1 + c_2}{3}$.

The expressions of the node DOFs $\bar{\mathbf{u}}_1^{(e)}$ and $\mathbf{u}_1^{(e)}$ in Fig.1:

$$\bar{\mathbf{u}}_1^{(e)} = \left[u_1^1, \frac{\partial u_1^1}{\partial x}, \frac{\partial^2 u_1^1}{\partial x^2}, u_1^2, \frac{\partial u_1^2}{\partial x}, \frac{\partial^2 u_1^2}{\partial x^2} \right]^T,$$

$$\mathbf{u}_1^{(e)} = \left[u_1^i, \frac{\partial u_1^i}{\partial x}, \frac{\partial^2 u_1^i}{\partial x^2}, \frac{\partial u_1^i}{\partial y}, \frac{\partial^2 u_1^i}{\partial x \partial y}, \frac{\partial^3 u_1^i}{\partial x^2 \partial y}, \frac{\partial^2 u_1^i}{\partial y^2}, \frac{\partial^3 u_1^i}{\partial x \partial y^2}, \frac{\partial^4 u_1^i}{\partial x^2 \partial y^2}, \frac{\partial u_1^i}{\partial z}, \frac{\partial^2 u_1^i}{\partial x \partial z}, \frac{\partial^3 u_1^i}{\partial x^2 \partial z}, \frac{\partial^2 u_1^i}{\partial y \partial z}, \frac{\partial^3 u_1^i}{\partial x \partial y \partial z}, \frac{\partial^4 u_1^i}{\partial x^2 \partial y \partial z}, \frac{\partial^3 u_1^i}{\partial y^2 \partial z}, \frac{\partial^4 u_1^i}{\partial x \partial y^2 \partial z}, \frac{\partial^5 u_1^i}{\partial x^2 \partial y^2 \partial z}, \frac{\partial^2 u_1^i}{\partial z^2}, \frac{\partial^3 u_1^i}{\partial x \partial z^2}, \frac{\partial^4 u_1^i}{\partial x^2 \partial z^2}, \frac{\partial^3 u_1^i}{\partial y \partial z^2}, \frac{\partial^4 u_1^i}{\partial x \partial y \partial z^2}, \frac{\partial^5 u_1^i}{\partial x^2 \partial y \partial z^2}, \frac{\partial^4 u_1^i}{\partial y^2 \partial z^2}, \frac{\partial^5 u_1^i}{\partial x \partial y^2 \partial z^2}, \frac{\partial^6 u_1^i}{\partial x^2 \partial y^2 \partial z^2} \right]^T, (i = 1, \dots, 8).$$

The shape function $\mathbf{N}(x)$ in Eq.8:

$$\mathbf{N}(x) = \begin{bmatrix} N_1^0(x) \\ N_1^1(x) \\ N_1^2(x) \\ N_1^0(x) \\ N_1^1(x) \\ N_1^2(x) \end{bmatrix}^T = \begin{bmatrix} \frac{5x^3}{8d_e^3} - \frac{15x}{16d_e} - \frac{3x^5}{16d_e^5} + \frac{1}{2} \\ \frac{5d_e}{16} - \frac{7x}{16} - \frac{3x^2}{8d_e} + \frac{5x^3}{8d_e^2} + \frac{16d_e^3}{16d_e^2} - \frac{3x^5}{16d_e^5} \\ \frac{d_e^2}{16} - \frac{d_e x}{16} - \frac{x^2}{8} + \frac{8d_e^2}{8d_e} + \frac{16d_e^3}{16d_e^2} - \frac{16d_e^4}{16d_e^5} \\ \frac{15x}{16d_e} - \frac{5x^3}{8d_e^3} + \frac{3x^5}{16d_e^5} + \frac{1}{2} \\ \frac{3x^2}{16d_e} - \frac{7x}{16} - \frac{5d_e}{8d_e} + \frac{5x^3}{8d_e^2} - \frac{16d_e^3}{16d_e^2} + \frac{3x^5}{16d_e^5} \\ \frac{8d_e}{d_e x} - \frac{16}{d_e^2} - \frac{16}{x^2} + \frac{8d_e^2}{x^3} - \frac{16d_e^3}{x^4} - \frac{16d_e^4}{x^5} \\ \frac{1}{16} + \frac{1}{16} - \frac{1}{8} - \frac{1}{8d_e} + \frac{1}{16d_e^2} + \frac{1}{16d_e^3} \end{bmatrix}.$$

References

- [1] B. Mace, Wave reflection and transmission in beams, *Journal of Sound and Vibration* 97 (1984) 237–246.
- [2] J.-M. Mencik, M. Ichchou, Multi-mode propagation and diffusion in structures through finite elements, *European Journal of Mechanics A/Solids* 24 (2005) 877–898.
- [3] S. Taleb, M. Sinapius, F. Boubenider, D. Schmidt, Experimental study of lamb waves propagation inside an impact damage in the size of the used wavelength, *Russian Journal of Nondestructive Testing* 56 (2) (2020) 141–150.
- [4] I. Herrero-Durá, A. Cebrecos, R. Picó, V. Romero-García, L. M. García-Raffi, V. J. Sánchez-Morcillo, Sound absorption and diffusion by 2d arrays of helmholtz resonators, *Applied Sciences* 10 (5) (2020) 1690.
- [5] H.-T. Thai, T. P. Vo, T.-K. Nguyen, T.-K. Nguyen, A review of continuum mechanics models for size-dependent analysis of beams and plates, *Composite Structures* 177 (2017) 196–219.
- [6] B. Zhang, H. Li, L. Kong, J. Wang, H. Shen, Strain gradient differential quadrature beam finite elements, *Computers & Structures* 218 (2019) 170–189.
- [7] J. Hamilton, W. Wolfer, Theories of surface elasticity for nanoscale objects, *Surface Science* 603 (9) (2009) 1284–1291.
- [8] V. A. Eremeyev, G. Rosi, S. Naili, Transverse surface waves on a cylindrical surface with coating, *International Journal of Engineering Science* 147 (2020) 103188.
- [9] S. El-Sapa, Effect of magnetic field on a microstretch fluid drop embedded in an unbounded another microstretch fluid, *European Journal of Mechanics-B/Fluids* 85 (2021) 169–180.
- [10] Y. Chen, J. D. Lee, Determining material constants in micromorphic theory through phonon dispersion relations, *International Journal of Engineering Science* 41 (8) (2003) 871–886.
- [11] X. Zeng, Y. Chen, J. D. Lee, Determining material constants in nonlocal micromorphic theory through phonon dispersion relations, *International journal of engineering science* 44 (18-19) (2006) 1334–1345.
- [12] T. Aksencer, M. Aydogdu, Levy type solution method for vibration and buckling of nanoplates using nonlocal elasticity theory, *Physica E: Low-dimensional Systems and Nanostructures* 43 (4) (2011) 954–959.
- [13] M. R. Barati, Vibration analysis of porous fg nanoshells with even and uneven porosity distributions using nonlocal strain gradient elasticity, *Acta Mechanica* 229 (3) (2018) 1183–1196.

- [14] R. E. Miller, V. B. Shenoy, Size-dependent elastic properties of nano-sized structural elements, *Nanotechnology* 11 (3) (2000) 139.
- [15] E. Kroner, Elasticity theory of materials with long range cohesive forces, *International Journal of Solids and Structures* 3 (1967) 731–742.
- [16] A. Muc, Non-local approach to free vibrations and buckling problems for cylindrical nano-structures, *Composite Structures* 250 (2020) 112541.
- [17] A. Eringen, Simple microfluids, *International Journal of Engineering Science* 2 (1964) 205–217.
- [18] A. Eringen, Linear theory of micropolar elasticity, *Journal of Applied Mathematics and Mechanics* 15 (1966) 909–923.
- [19] M. E. Gurtin, A. I. Murdoch, A continuum theory of elastic material surfaces, *Archive for rational mechanics and analysis* 57 (4) (1975) 291–323.
- [20] L. Li, R. Lin, T. Y. Ng, Contribution of nonlocality to surface elasticity, *International Journal of Engineering Science* 152 (2020) 103311.
- [21] M. Lazar, G. A. Maugin, E. C. Aifantis, Dislocation in second strain gradient elasticity, *International Journal of Solids and Structures* (2006) 1787–1817.
- [22] M. Arefi, M. Kiani, T. Rabczuk, Application of nonlocal strain gradient theory to size dependent bending analysis of a sandwich porous nanoplate integrated with piezomagnetic face-sheets, *Composites Part B: Engineering* 168 (2019) 320–333.
- [23] G. Fu, S. Zhou, L. Qi, On the strain gradient elasticity theory for isotropic materials, *International Journal of Engineering Science* 154 (2020) 103348.
- [24] M. M. S. Fakhraabadi, Prediction of small-scale effects on nonlinear dynamic behaviors of carbon nanotube-based nano-resonators using consistent couple stress theory, *Composites Part B: Engineering* 88 (2016) 26–35.
- [25] H. Shodja, A. Goodarzi, M. Delfani, H. Haftbaradaran, Scattering of an anti-plane shear wave by an embedded cylindrical micro-/nano-fiber within couple stress theory with micro inertia, *International Journal of Solids and Structures* 58 (2015) 73–90.
- [26] S. J. Behrouz, O. Rahmani, S. A. Hosseini, On nonlinear forced vibration of nano cantilever-based biosensor via couple stress theory, *Mechanical Systems and Signal Processing* 128 (2019) 19–36.
- [27] R. D. Mindlin, Micro-structure in linear elasticity, *Archive for Rational Mechanics and Analysis* 16 (1964) 51–78.
- [28] B. Karami, M. Janghorban, A. Tounsi, Variational approach for wave dispersion in anisotropic doubly-curved nanoshells based on a new nonlocal strain gradient higher order shell theory, *Thin-Walled Structures* 129 (2018) 251–264.
- [29] R. D. Mindlin, Second gradient of strain and surface tension in linear elasticity, *International Journal of Solids and Structures* (1965) 147–438.
- [30] N. M. Cordero, S. Forest, E. P. Busso, Second strain gradient elasticity of nano-objects, *Journal of the Mechanics and Physics of Solids* 97 (2016) 92–124.
- [31] Z.-Q. Tan, Y.-C. Chen, Size-dependent electro-thermo-mechanical analysis of multilayer cantilever microactuators by joule heating using the modified couple stress theory, *Composites Part B: Engineering* 161 (2019) 183–189.
- [32] A. M. Dehrouyeh-Semnani, M. Nikkiah-Bahrami, The influence of size-dependent shear deformation on mechanical behavior of microstructures-dependent beam based on modified couple stress theory, *Composite Structures* 123 (2015) 325–336.
- [33] X. Yu, A. Maalla, Z. Moradi, Electroelastic high-order computational continuum strategy for critical voltage and frequency of piezoelectric nems via modified multi-physical couple stress theory, *Mechanical Systems and Signal Processing* 165 (2022) 108373.
- [34] H. M. Shodja, F. Ahmadpoor, T. A., Calculation of the additional constants for fcc materials in second strain gradient elasticity: behavior of a nano-size bernoulli-euler beam with surface effects, *Applied Mechanics* 72 (2) (2010) 021008.
- [35] S. Momeni, M. Asghari, The second strain gradient functionally graded beam formulation, *Composite Structures* 188 (2018) 15–24.
- [36] C.W.Lim, G.Zhang, J.N.Reddy, A higher-order nonlocal elasticity and strain gradient theory and its applications in wave propagation, *Journal of the Mechanics and Physics of Solids* 78 (2015) 298–313.
- [37] D. D. Domenico, H. Askes, Stress gradient, strain gradient and inertia gradient beam theories for the simulation of flexural wave dispersion in carbon nanotubes, *Composites Part B: Engineering* 153 (2018) 285–294.
- [38] G. Zhu, A. Zine, C. Droz, M. Ichchou, Wave transmission and reflection analysis through complex media based on the second strain gradient theory, *European Journal of Mechanics / A Solids* (2021).
- [39] J. Torabi, R. Ansari, M. Darvizeh, A c1 continuous hexahedral element for nonlinear vibration analysis of nano-plates with circular cutout based on 3d strain gradient theory, *Composite Structures* 205 (2018) 69–85.
- [40] J. Torabi, R. Ansari, M. Bazdid-Vahdati, M. Darvizeh, Second strain gradient finite element analysis of vibratory nanostructures based on the three-dimensional elasticity theory, *Iranian Journal of Science and Technology, Transactions of Mechanical Engineering* 44 (2020) 631–645.
- [41] D. Mahapatra, S. Gopalakrishnan, A spectral finite element for analysis of wave propagation in uniform composite tubes, *Journal of Sound and Vibration* 268 (2003) 429–463.
- [42] S. Finnveden, M. Fraggstedt, Waveguide finite elements for curved structures, *Journal of Sound and Vibration* 312 (2008) 644–671.
- [43] J. M. Mencik, M. N. Ichchou, Wave finite elements in guided elastodynamics with internal fluid, *International Journal of Solids and Structures* 44 (2007) 2148–2167.
- [44] C. Droz, J. P. Lainé, M. N. Ichchou, G. Inquiété, A reduced formulation for the free-wave propagation analysis in composite structures, *Composite Structures* 113 (2014) 134–144.
- [45] F. Errico, M. Ichchou, S. De Rosa, F. Franco, O. Bareille, Investigations about periodic design for broadband increased sound transmission loss of sandwich panels using 3d-printed models, *Mechanical Systems and Signal Processing* 136 (2020) 106432.
- [46] R. Singh, C. Droz, M. Ichchou, F. Franco, O. Bareille, S. De Rosa, Stochastic wave finite element quadratic formulation for periodic media: 1d and 2d, *Mechanical Systems and Signal Processing* 136 (2020) 106431.
- [47] D. Mead, A general theory of harmonic wave propagation in linear periodic systems with multiple coupling, *Journal of Sound and Vibration* 27 (1973) 235–260.
- [48] M. Ichchou, F. Bouchoucha, M. B. Souf, O. Dessombz, M. Haddar, Stochastic wave finite element for random periodic media through first-order perturbation, *Computer Methods in Applied Mechanics and Engineering* 200 (41-44) (2011) 2805–2813.
- [49] D. Duhamel, B. R. Mace, M. Brennan, Finite element analysis of the vibrations of waveguides and periodic structures, *Journal of Sound and Vibration* 294 (2006) 205–220.
- [50] M. Ichchou, J.-M. Mencik, W. Zhou, Wave finite elements for low and mid-frequency description of coupled structures with damage, *Computer methods in applied mechanics and engineering* 198 (15-16) (2009) 1311–1326.

- [51] B. Yang, C. Droz, A. Zine, M. Ichchou, Dynamic analysis of second strain gradient elasticity through a wave finite element approach, *Composite Structures* 263 (2021).
- [52] B. Yang, A. Zine, C. Droz, M. Ichchou, Two-dimensional periodic structures modeling based on second strain gradient elasticity for a beam grid, *International Journal of Mechanical Sciences* (2022).
- [53] H. Reda, I. Goda, J. Ganghoffer, G. l'Hostis, H. Lakiss, Dynamical analysis of homogenized second gradient anisotropic media for textile composite structures and analysis of size effects, *Composite Structures* 161 (2017) 540–551.
- [54] C. Droz, R. F. Boukadia, M. Ichchou, W. Desmet, Diffusion-based design of locally resonant sub-systems using a reduced wave finite element framework, *Proceedings of ISMA-International Conference on Noise and Vibration Engineering* (2018) 3071–3083.
- [55] L. Placidi, G. Rosi, I. Giorgio, A. Madeo, Reflection and transmission of plane waves at surfaces carrying material properties and embedded in second-gradient materials, *Mathematics and Mechanics of Solids* 19 (5) (2014) 555–578.
- [56] E. Barchiesi, A. Misra, L. Placidi, E. Turco, Granular micromechanics-based identification of isotropic strain gradient parameters for elastic geometrically nonlinear deformations, *ZAMM-Journal of Applied Mathematics and Mechanics/Zeitschrift für Angewandte Mathematik und Mechanik* 101 (11) (2021) e202100059.
- [57] W. P. Davey, Precision measurements of the lattice constants of twelve common metals, *Physical Review* 25 (6) (1925) 753.
- [58] J. Q. Zhao, P. Zeng, B. Pan, Improved hermite finite element smoothing method for full-field strain measurement over arbitrary region of interest in digital image correlation, *Optics and Lasers in Engineering* 50 (2012) 1662–1671.
- [59] I. Bennamia, A. Badereddine, T. Zebbiche, Measurement of vibrations of composite wings using high-order finite element beam, *Journal of Measurements in Engineering* 6 (2018) 143–154.
- [60] S. Khakalo, J. Niiranen, Form ii of mindlin's second strain gradient theory of elasticity with a simplification: For materials and structures from nano- to macro-scales, *European Journal of Mechanics / A Solids* 71 (2018) 292–319.
- [61] V. Balobanov, J. Niiranen, Locking-free variational formulations and isogeometric analysis for the timoshenko beam models of strain gradient and classical elasticity, *Computer Methods in Applied Mechanics and Engineering* 339 (2018) 137–159.
- [62] V. Tarasov, Lattice model with nearest-neighbor and next-nearest-neighbor interactions for gradient elasticity, *Discontinuity, Nonlinearity, and Complexity* 4 (2015) 11–23.
- [63] M. Asghari, S. A. Momeni, R. Vatankhah, The second strain gradient theory-based timoshenko beam model, *Journal of Vibration and Control* 23 (13) (2015) 2155–2166.
- [64] S. A. Momeni, M. Asghari, The second strain gradient functionally graded beam formulation, *Composite Structures* 188 (2018) 15–24.
- [65] G. Rosi, L. Placidi, N. Auffray, On the validity range of strain-gradient elasticity: a mixed static-dynamic identification procedure, *European Journal of Mechanics-A/Solids* 69 (2018) 179–191.
- [66] K. Graff, *Wave Motion in Elastic Solids*, Oxford University Press, London, 1991, Ch. Longitudinal waves in the rods, pp. 75–130.
- [67] Z. Guang, D. Christophe, Z. Abdelmalek, M. Ichchou, Wave propagation analysis for a second strain gradient rod theory, *Chinese Journal of Aeronautics* 33 (10) (2020) 2563–2574.
- [68] S. Ahsani, R. Boukadia, C. Droz, C. Claeys, E. Deckers, W. Desmet, Diffusion based homogenization method for 1d wave propagation, *Mechanical Systems and Signal Processing* (2020).